

I give permission for public access to my thesis and for copying to be done at the discretion of the archives' librarian and/or the College library.

Signature Date

A *DROSOPHILA MELANOGASTER* MODEL FOR UNDERSTANDING
HUMAN SPORADIC INCLUSION BODY MYOSITIS

By

Wilmina Nhoue'deh Landford

A Paper Presented to the
Faculty of Mount Holyoke College in
Partial Fulfillment of the Requirements for
the Degree of Bachelors of Arts with
Honor

Department of Biological Sciences

South Hadley, MA 01075

May, 2008

This paper was prepared
under the direction of
Professor Craig Woodard
For eight credits.

Much dreaming and many words are meaningless. Therefore stand in awe of God
- Ecclesiastes 5:7

ACKNOWLEDGMENTS

First and foremost, I would like to thank God for giving me so many blessings in life. I would like to thank Him for blessing me with certain people in my life who have helped me become the woman that I am now. I would like to thank Professor Craig Woodard for his commitment in being an advisor, role model, and inspirational leader. Professor Woodard has given me the motivation to continue on with my aspirations by believing in me and dedicating his time to make sure I succeed. I would like to thank Marian Rice for spending the time to help me with my results and TEM use. I would like to thank Professor Jeff Knight for being part of my thesis committee and for giving me advice on questions that my have caused obstacles for me. I would like to thank Professor Sheila Browne for being part of my committee and for being blessing when I've needed help.

I would like to thank my parents for being my foundation, and for being my support as I reach towards the stars. Their sacrifices have allowed me to pursue my dreams. I would like to thank my friends, who are my sisters, for the emotional and spiritual support throughout the years at Mount Holyoke. I would like to thank all those professors who have supported my hunger for knowledge.

TABLE OF CONTENTS

	Page No.
List of Figures	vi
Abstract	ix
Introduction	1
Sporadic-Inclusion Body Myositis.....	1
Pathological Events leading to the Pathogenesis of sIBM	2
Amyloid-Precursor Protein and its Proteolytic fragments	8
Amyloid-precursor protein in Cell Metabolism	9
Proteolytic Processing of APP	10
γ -secretase cleavage	14
Presenilin and its role in APP proteolysis	16
<i>Drosophila</i> as a model organism	19
Expression of APP and presenilin in <i>Drosophila melanogaster</i>	23
Mitochondrial defects as a phenotypic marker.....	25
Aim of my research	28
Materials and Methods	30
UAS-Gal4 system	30
Crosses to Generate Experimental Genotypes.....	31
Climbing assays	34
PsnE280 lines	34
PsnL237 lines	34
Flight assays	35
Transmission Electron Microscopy.....	35
PsnE280 lines	35

PsnL237 lines	35
Results	37
Climbing Assays	37
PsnE280 lines	37
PsnL237 lines	44
Flight Assays.....	50
PsnE280 lines	50
PsnL237 lines	57
Transmission Electron Microscopy	64
Discussion	68
Use of Climbing Assays to evaluate hAPP and mutant presenilin Interaction.....	70
Flight Assays to evaluate muscle activity.....	75
Transmission Electron Microscopy to examine changes Muscle fiber.....	76
Conclusion.....	78
Literature Cited	79

LIST OF FIGURES

	Page No.
1. Mechanism for the pathogenesis of sporadic-Inclusion Body Myositis	6
2. Histological features in cross-sections of muscle biopsies in patients with sporadic Inclusion Body Myositis	7
3. Proteolytic processing of APP by the three secretases, α -, β -, and γ -secretase	12
4. Schematic diagram of the proteolytic processing of APP.....	13
5. Life cycle of <i>Drosophila melanogaster</i>	22
6. Transmission electron micrographs of wildtype and hAPP-expressing flight muscles	28
7. Stock lines using the UAS and Dmef-Gal4 system to express the appropriate genotypes in muscle cells	33
8. The w^{1118} control standard and siliconized-vial climbing assay results	41
9. hAPP-expressing standard and siliconized-vial climbing assay results	41
10. $PsnE^{280}$ standard and siliconized-vial climbing assay results	42
11. Flies coexpressing hAPPxPsnE ²⁸⁰ standard and siliconized-vial climbing assay results.....	42
12. Standard climbing assay of $PsnE^{280}$, hAPPxPsnE ²⁸⁰ hAPP and w^{1118}	43
13. Siliconized climbing assay of $PsnE^{280}$, hAPPxPsnE ²⁸⁰ , hAPP and w^{1118}	43
14. The w^{1118} standard and siliconized-vial climbing assay results	47
15. hAPP-expressing standard and siliconized-vial	

climbing assay results.....	47
16. <i>PsnL</i> ²³⁷ standard and siliconized-vial climbing assay results.....	48
17. Flies coexpressing <i>hAPPxPsnL</i> ²³⁷ standard and siliconized-vial climbing assay results.....	48
18. Standard climbing assay of <i>PsnL</i> ²³⁷ , <i>hAPPxPsnL</i> ²³⁷ , <i>hAPP</i> and <i>w</i> ¹¹¹⁸	49
19. Siliconized climbing assay of <i>PsnL</i> ²³⁷ , <i>hAPPxPsnL</i> ²³⁷ , <i>hAPP</i> and <i>w</i> ¹¹¹⁸	49
20. Flight Assay Result of the <i>w</i> ¹¹¹⁸ controls in Standard and Siliconized Vials	54
21. Flight Assay Result of <i>hAPP</i> – expressing flies in Standard and Siliconized Vials.....	54
22. Flight Assay Result of <i>PsnE</i> ²⁸⁰ in Standard and Siliconized Vials.....	55
23. Flight Assay Result of <i>hAPPxPsnE</i> ²⁸⁰ in Standard and Siliconized Vials.....	55
24. Standard flight assay of <i>PsnE</i> ²⁸⁰ , <i>hAPPxPsnE</i> ²⁸⁰ , <i>hAPP</i> and <i>w</i> ¹¹¹⁸	56
25. Siliconized flight assay of <i>PsnE</i> ²⁸⁰ , <i>hAPPxPsnE</i> ²⁸⁰ , <i>hAPP</i> and <i>w</i> ¹¹¹⁸	56
26. Flight Assay Result of the <i>w</i> ¹¹¹⁸ controls in Standard and Siliconized Vials.....	61
27. Flight Assay Result of <i>hAPP</i> -expressing flies in Standard and Siliconized Vials	61
28. Flight Assay Result of <i>PsnL</i> ²³⁷ in Standard and Siliconized Vials.....	62
29. Flight Assay Result of flies coexpressing <i>hAPPxPsnL</i> ²³⁷ in Standard and Siliconized-Vial flies.....	62
30. Standard climbing assay of <i>PsnL</i> ²³⁷ , <i>hAPPxPsnL</i> ²³⁷ ,	

<i>hAPP</i> and w^{1118}	63
31. Standard climbing assay of $PsnL^{237}$, $hAPPxPsnL^{237}$, <i>hAPP</i> and w^{1118}	63
32. Transmission electron micrograph of w^{1118} , $PsnL^{237}$, <i>hAPP</i> , and $hAPPxPsnL^{237}$ at 1 week.....	66
33. Transmission electron micrograph of w^{1118} , $PsnL^{237}$, <i>hAPP</i> , and $hAPPxPsnL^{237}$ at 3 weeks.....	67

ABSTRACT

Sporadic-Inclusion Body Myositis (s-IBM) is a muscle disease that is characterized by a slow-onset of weakness and atrophy in muscles of certain parts of the body. A specific protein present in patients with s-IBM called amyloid precursor protein (APP) and certain proteolytic fragments of APP serve as primary agents in pathogenesis. In order to understand the role of proteins responsible for pathogenesis, transgenic flies were bred to express wildtype human APP (hAPP) and presenilin. The intrinsic attributes of presenilin in the proteolytic processing of APP have adverse effects if alterations occur. A mutation in presenilin leads to an increase in A β production, resulting in the formation of aggregates, which triggers necrosis of the muscle cells. It was the aim of the study to investigate the effect of proteolytic fragments on sIBM. The accumulation of hAPP and proteolytic fragments A β 40 and/or A β 42 are a causative factor in sIBM and amyloid-related diseases such as Alzheimer's disease. These abnormal fragments are produced by transmembrane proteases, α -, β -, and γ -secretase. Alterations in secretase activity have been found to be a prime factor responsible for the production of these aggregates. Two proteins important in age-dependent neurodegeneration in the nervous system are the β -secretase protein BACE and presenilin, found in the γ -secretase protease complex. The goal of my research was to focus on the genetic factors that influence muscle degeneration in patients with sporadic-Inclusion Body Myositis (s-IBM) by exploring the interaction of presenilin in APP proteolysis in transgenic *D. melanogaster*. In my research I focused on behavioral changes due to the coexpression of mutant presenilin alleles with human APP in muscle cells. I hypothesized that the expression of mutant presenilin will affect the structure and function of muscles in *D. melanogaster* and therefore, exacerbate the symptoms of sporadic-Inclusion Body Myositis. Any stress that results in the onset of degeneration suggests that pathogenesis is muscle activity-dependent. To confirm that the presence of a mutation in presenilin genes causes degeneration in skeletal muscles, flies coexpressing mutant presenilin and hAPP were subjected to climbing and flight assays. The results allowed us to find differences among the wildtype and mutants so that conclusions could be made on the effect of hAPP on behavior. The significance of this work is to allow us to identify candidate targets for therapeutic intervention for the treatment of s-IBM.

INTRODUCTION

Sporadic Inclusion Body Myositis

Sporadic-Inclusion Body Myositis (sIBM) is a myopathy that affects the muscles of distal and proximal limbs and results in the slow-onset of weakness and atrophy. Patients with sIBM complain of weakness in facial and pharyngeal muscles as well as weakness in the deep flexor muscles of their fingers. The emergence of these clinical phenotypes is common in patients of age 50 years and older and affects men slightly more frequently than women (Dalakas, 2006). This rare disease affects less than 200,000 people in the US population (Adams *et al.*, 2000). The acquired, adult-onset of inflammation in sporadic-Inclusion Body Myositis is distinct from hereditary-Inclusion Body Myositis, where symptoms commence at childhood and lack the myopathic features of inflammation in the muscles (Adams *et al.*, 2000.).

As an age-related muscle disease, sIBM has been frequently misdiagnosed as polymyositis and given ineffective treatment. There is no beneficial treatment for s-IBM. Indication of sIBM is characterized by inflammation in the endomysium, muscle fiber necrosis, elevation of serum muscle enzymes, and a degree of weakness (Dalakas, 2006). Muscle biopsies show the presence of mononuclear cell inflammation, vacuolated muscle fibers containing paired helical filaments, and 6- to 10-nm fibrils that accumulate in the cell (Askanas and Engel, 2007). The apparent stress found in the limbs is characterized by the

predisposition of aging muscle fibers to muscle fiber necrosis and contribution to vacuolar degeneration, leading to disease progression. Within vacuoles localized in the cells, there is an occurrence of abnormal accumulation of insoluble protein called amyloid-related proteins (Wolfe *et al.*, 1999).

Myopathic features that lead to the progression of sIBM are acquired by lymphocytic infiltrates invading non-vacuolated fibers, vacuolar degeneration, and the expression of several potentially toxic proteins (Dalakas, 2006). The toxic proteins found in sIBM are insoluble amyloid-related proteins that form aggregates and which account for the pathological events that lead to muscle degeneration and weakness in sIBM. The accumulation of amyloid-related proteins is also known as inclusion bodies, which define the name of the disease. Several of these amyloid-related diseases include Alzheimer's disease, Amyotrophic Lateral Sclerosis, Huntington Disease, Diabetes mellitus, and Parkinson's disease (Jayaraman *et al.*, 2008).

Pathological Events leading to pathogenesis of sIBM

The cascade of events that lead to the pathogenesis of sIBM is triggered by an unknown cause resulting in an autoimmune inflammatory event and degenerative event. Muscle biopsies from patients with sIBM show non-vacuolated muscle fibers invaded by cytotoxic T cells, whereas invasion of vacuolated fibers is scarce (Dalakas, 2006). In the autoimmune event, T-cells invade muscle fibers

abnormally expressing MHC class I molecules. In the degenerative event, vacuoles appear in the muscles, deposits of amyloid-related proteins are scattered in the cells, and filamentous inclusions of abnormal proteins disrupt the normal functioning of the cell, thus inducing apoptosis (Tabaton and Tamagno, 2007). The two events are believed to occur simultaneously, although two major arguments suggest that one event occurs slightly before the other. Dalakas (2006) proposes that the inflammation present in the autoimmune event is the primary cause following the degeneration of muscle fibers whereas other researchers, such as Askanas (2001) argue that biological changes associated with aging found in patients with sIBM, who are typically older patients may be eliciting the lymphocytic inflammation.

In the autoimmune event, the expression of MHC class I molecules accelerates the degenerative process of the cells (fig. 1). Conventionally, muscle fibers do not express MHC class I molecules on their surface. In abnormal circumstances, such as sIBM, the MHC class I molecules are expressed ubiquitously on all muscle cells including non-vacuolated muscle fibers (Dalakas, 2006). The presence of vacuoles in the muscle fibers is the main cause for the upregulation of MHC class I molecules, which indicates that other factors may be the cause of MHC class I expression on non-vacuolated muscle fibers. The assembly of MHC class I molecules is regulated by a multi-protein complex in the endoplasmic reticulum (ER) called the loading complex (Antoniou *et al.*, 2003). The process begins with the association of a heavy glycoprotein with $\beta 2$

microglobulin forming an unstable heterodimer complex that matures only when it binds to an antigenic peptide (Antoniou *et al.*, 2003). Antigenic peptides are generated by the proteasome in the cytoplasm and then translocated by the transporter associated with antigen processing (TAP) into the lumen of the ER (Antoniou *et al.*, 2003). The peptide ultimately loads onto the MHC class I molecule and the complex is then transported to the cell surface. In sIBM, the production of MHC class I molecules is driven by an unidentified antigen. Folded proteins are usually soluble and can localize within a cell without difficulty. Misfolded proteins are insoluble and must be degraded and therefore are transported into a proteasome for degradation. If high levels of misfolded proteins occur, the degradative capacity is exceeded and accumulation occurs (Needham and Mastaglia, 2008). An inability for antigenic peptides to undergo a conformational change and bind to the MHC class I molecules results in an overload of MHC class I molecules in the endoplasmic reticulum. This leads to ER stress and protein misfolding (Dalakas, 2006). Possible triggering factors could be viruses that may alter the environment of the aging muscle fibers and therefore initiate the clonal expansion of T-cells and T-cell mediated immunity via the perforin pathway. The cytokines released in the environment upregulate MHC class I molecules that are confined in the ER resulting in an overload of the ‘MHC-peptide-loading-complex’ and an ER stress response (Dalakas, 2006). Subsequently, an accumulation of amyloid-related glycoproteins along with the activation of transcription factor NF κ B promote the expression of additional

cytokines therefore inducing a self-sustaining inflammatory response (Dalakas, 2006). Another contributing factor to the accumulation of amyloid-related protein is impaired proteosomal function that is known to occur with aging. The continual processing of mutant and misfolded proteins can damage the proteosomal from further processing, resulting in accumulations of misfolded proteins (Needham and Mastaglia, 2008).

Modifications associated with aging result in damage and interference in cell metabolism. In addition, the breakdown of tolerance in the immune system could contribute to the derangement of T-cells to recognize “self” and “foreign” antigens (Askanas and Engel, 2007). The final product, aggregations of amyloid, contributes to the deteriorating cellular environment by inducing necrosis and therefore degeneration of the muscle fibers. The degenerative process of sIBM can be analyzed by using methods such as muscle biopsies and electromyography to examine any stresses in the muscle tissue. Degeneration in the muscle cells can be characterized by the presence of vacuoles, fiber amyloid inclusions, and oxidative stress proteins (Askanas and Engel, 2007). Common types of intracellular inclusions are A β or phosphorylated tau. The accumulation of these protein aggregates consequentially lead to intracellular inclusions from unusual binding of hydrophobic surfaces in misfolded polypeptides (Askanas and Engel, 2007). Analysis of muscle biopsy samples from patients reveals the presence of amyloid precursor proteins (APP) and its proteolytic fragments, which play an integral role in the degeneration of muscle cells (fig. 2).

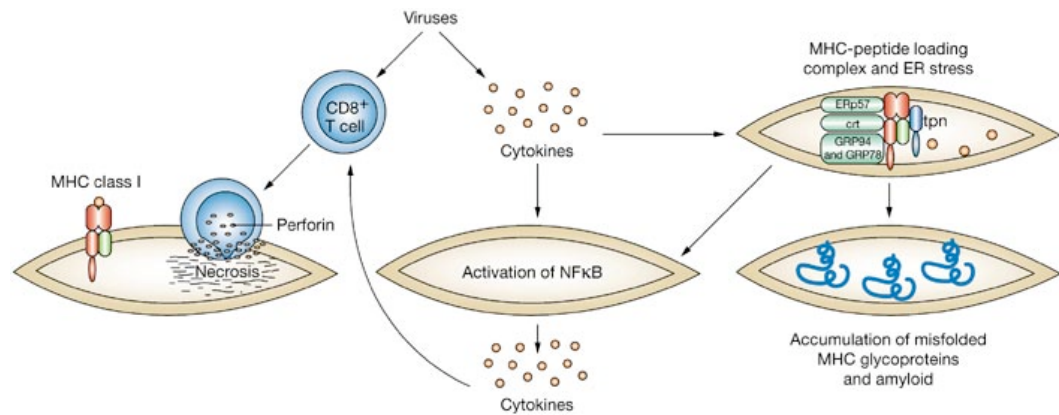


Figure 1. Mechanism for the pathogenesis of sporadic-Inclusion Body Myositis

Viral triggers lead to clonal expansion of CD⁸⁺ T cells and T-cell-mediated cytotoxicity via the perforin pathway. The released cytokines upregulate MHC class I molecules and increase levels of the MHC-peptide loading complex, because the abundance of generated peptides cannot be conformationally assembled with the MHC to exit the ER. As a result, there is an ER stress response, which leads to activation of the transcription factor NFκB and accumulation of misfolded MHC glycoproteins, including amyloid-related proteins. Both NFκB and amyloid-related misfolded proteins promote the expression of inflammatory mediator genes for cytokines, the products of which further stimulate the MHC-CD⁸ complex, resulting in a self-sustaining inflammatory response, thereby closing the loop between inflammation and degeneration (Dalakas 2006).

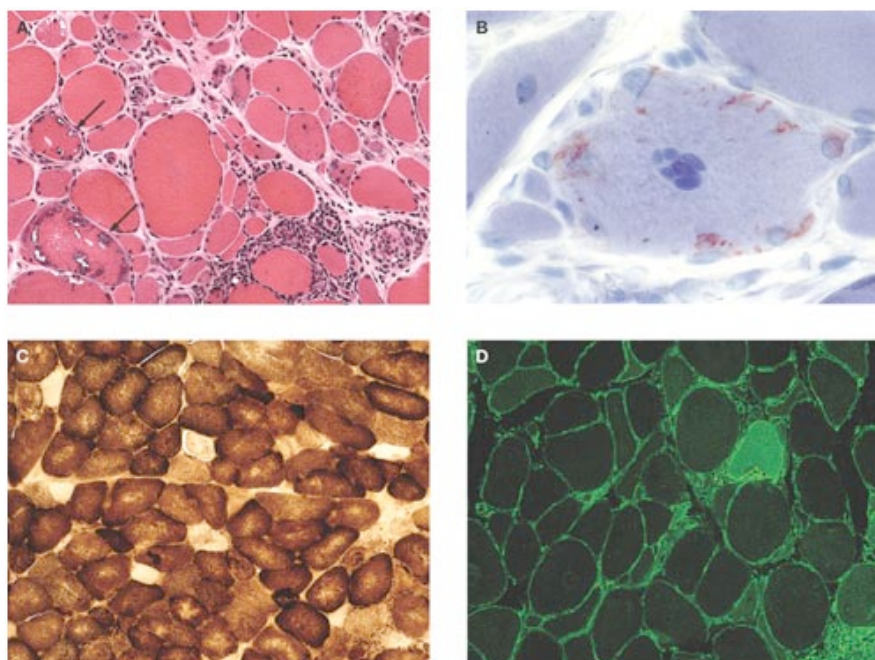


Figure 2. Histological features in cross-sections of muscle biopsies in patients with sporadic Inclusion Body Myositis

(A) Inflammation and vacuoles. Note endomysial inflammation, with lymphocytes invading non-necrotic, healthy-appearing muscle fibers, and 'red-rimmed' vacuoles in two muscle fibers (arrows) not invaded by inflammatory cells. If the course of the same vacuolated fibers is followed at considerable length in longitudinal sections, they remain devoid of autoinvasive inflammatory T cells. **(B)** Intracellular deposits of amyloid easily identified with crystal violet stain on frozen sections. **(C)** Scattered cytochrome-oxidase-negative fibers, indicative of abnormal mitochondrial function. **(D)** Strong major histocompatibility complex class I expression (green) in all fibers, regardless of whether they are invaded by T cells (Dalakas, 2006).

Amyloid-Precursor Protein and its Proteolytic fragments

The production of senile plaques present in Alzheimer's disease and the aggregates in sIBM are the result of β -amyloid peptides ($A\beta$) (Jayaraman *et al.*, 2008). $A\beta$ peptides vary in size ranging from 39-43 amino acids long (Turner *et al.*, 2003). Although $A\beta$ can exist in the cells as a monomer, dimer, and oligomer they exist prevalently as dimers and are produced intracellularly and then secreted (Turner *et al.*, 2003). As an important component of normal cell metabolism, elevations in $A\beta$ levels due to disease progression exhibit adverse effects (Turner *et al.*, 2003). Preliminary studies have shown that accumulation of amyloid precursor proteins and its proteolytic fragments, $A\beta$ s, is primarily responsible for the pathogenesis of sIBM (Schwartz and Woodard, unpublished).

These physiological effects result in cell damage and ultimately necrosis of the cells. Electron microscopy confirms the presence of insoluble intracellular inclusions with amyloid-like features (Wolfe *et al.*, 1999). The degenerative features thus create a correlation with $A\beta$ deposition in sIBM, which has been linked to genes that affect the processing of $A\beta$ from APP. In addition, mutations in these proteins involved with processing of APP have been identified as a risk factor for developing sIBM and are thus believed to interact with APP and $A\beta$. Inclusion bodies found in sIBM are closely related to the aggregations found in the brains of Alzheimer's patients. Similar features are found in Huntington disease, and Parkinson's disease (Askanas and Engel, 2007). These aggregations in the cells are intensively toxic to neurons, myocytes, endothelial cells, and

erythrocytes (Jayaraman *et al.*, 2008). As a result, the degenerative process is a byproduct of the toxic effects of A β deposition.

Amyloid-precursor protein in Cell Metabolism

The complexity of the amyloid precursor protein (APP) has led researchers to fully analyze its role in development and homeostasis in the body. APP is a type I transmembrane glycoprotein sequentially cleaved to generate the amyloid- β (A β) peptide found in the inclusions of sIBM (Tabaton and Tamagno, 2007). As a single membrane-spanning protein, APP possesses a large extracellular N-terminus and a small intracellular C-terminus (Tabaton and Tamagno, 2007). In mammals, APP along with APLP1 and APLP2 (amyloid precursor-like proteins) are part of a protein family (Fossgreen *et al.*, 1998). The APP gene can be found on chromosome 21 and is ubiquitously expressed throughout the body including epithelia, glia, and neurons in the brain (Wolfe *et al.*, 1999).

Three isoforms, APP770, APP751, APP695, are derived from alternative splicing of APP pre-mRNA and are vicariously processed further by glycosylation and specific proteolytic cleavage (Turner *et al.*, 2003). The fragments generated through processing of APP become contributors to cell adhesion, intercellular communication, and membrane-nucleus signaling (Turner *et al.*, 2003). The primary isoform produced in the brain is APP695, which is accountable for the pathogenesis of Alzheimer's disease (Turner *et al.*, 2003). APP is localized

primarily in membranous structures such as the endoplasmic reticulum, golgi compartments, and neurons in the brain (Turner *et al.*, 2003). Once APP reaches the cell's surface, it is carried back into the cell by lysosomes where it encounters processing (Turner *et al.*, 2003).

Proteolytic Processing of APP

The two main sites of proteolytic processing for APP are the golgi and cell surface (Turner *et al.*, 2003). APP is processed by three different proteases called α -, β -, and γ -secretase, as shown on Figure 3 (Selkoe, 2001). Sequentially, β -secretase and α -secretase occur close to the membrane following a cleavage within the transmembrane domain by γ -secretase (Turner *et al.*, 2003). The final cleavage of APP results in the fabrication of A β peptides and other proteolytic fragments found in muscle cells (Tandon and Fraser., 2002). The enzymatic activity of these secretases is localized in the trans-golgi network of the cells (Turner *et al.*, 2003). In order for cleavage of the membrane-spanning receptor to occur, α -secretase takes on the role of cleaving the protein on the cell surface (Wolfe et al., 1999). The pathway involving α -secretase is known as the non-amyloidogenic pathway and is responsible for the default secretory pathway. β -secretase is a transmembrane aspartic protease composed of two enzymes, BACE and BACE2, that cleave at the β -site (Nunan and Small, 2000). The third

protease, γ -secretase, is an integral membrane protein that determines the final size of its substrates. APP proteolysis begins with β -secretase cleavage by BACE, which takes place outside the membrane in the extracellular domain near the transmembrane region of APP (Madsen et al., 2007). β -secretase cleaves APP at the N-terminus of the A β peptide producing soluble APP called sAPP β (Tabaton and Tamagno, 2007). The remaining strand is a 99-residue membrane-associated C-terminal fragment, C99 (Wolfe et al., 1999). α -secretase, comprised of ADAM10 and TACE, cleaves APP close to the membrane-spanning domain yielding sAPP α and an 83-residue membrane-associated C-terminal fragment, C83 (Turner *et al.*, 2003). Ultimately, the remaining residues C99 and C83 become substrates for γ -secretase (Tabaton and Tamagno, 2007). C99 is processed by γ -secretase resulting in a 4-kDa A β peptide while C83, a 3-kDa N-terminally truncated form of A β forms p3 (Wolfe et al., 1999). The cascade of sequential cleavages liberates A β peptides that range from 39-43 peptides long (Thinakaran, 1999). A β 42 is primarily generated through two protease cleavages from β - and γ -secretase (Madsen et al., 2007). Elevated levels of A β 42 are more common because of the peptide's ability to aggregate better than A β 40 (fig. 4). Irregularities and accumulations of A β peptides are an early feature in sIBM (Tabaton and Tamagno, 2007).

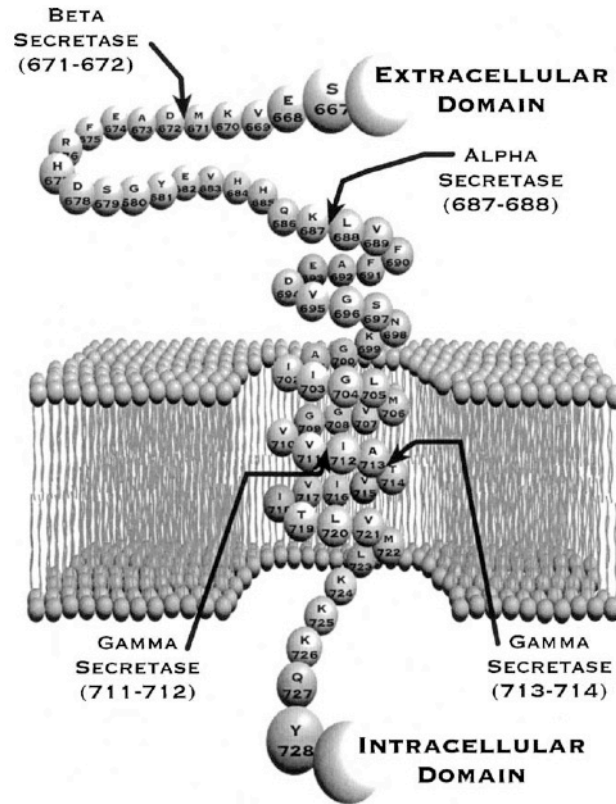


Figure 3. Proteolytic processing of APP by the three secretases, α -, β -, and γ -secretase

The $A\beta_{1-40}$ fragment, generated by β - and γ -cleavage, comprises residues 672-711 of APP770 while the amyloid β_{1-42} fragment spans residues 672-713. The p3 fragment, generated by α - and γ -cleavage spans residues residues 688-711 and 713. The helical region of the transmembrane domain extends past the alpha cleavage site and is important in secretase recognition (Turner *et al.*, 2003)

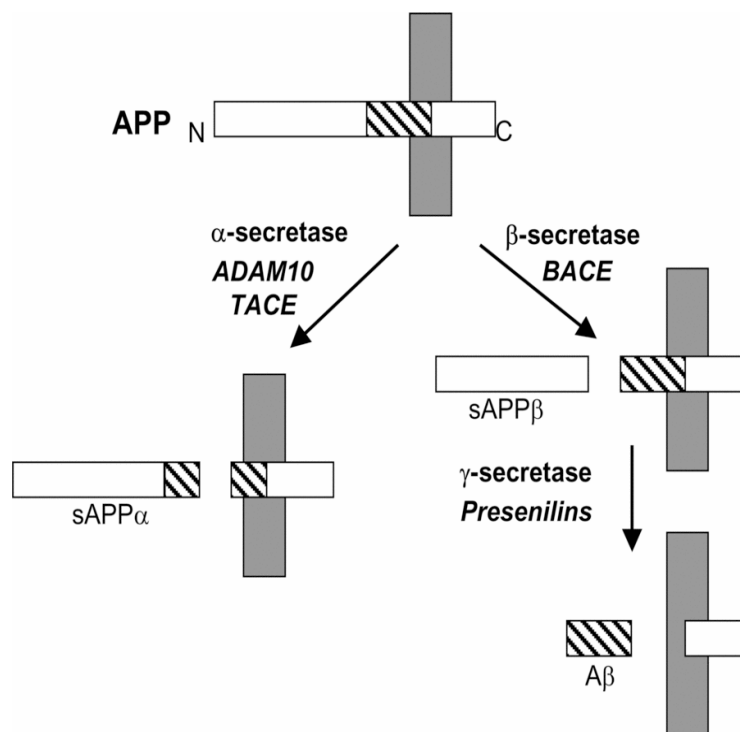


Figure 4. Schematic diagram of the proteolytic processing of APP

APP is a type I integral membrane protein (white rectangle) with the A β domain shown as the crosshatched region. The membrane is represented by the grey-shaded rectangle. In the non-amyloidogenic pathway, APP is cleaved within the A β domain by α -secretase, predominantly ADAM10 and TACE, to release the soluble ectodomain fragment sAPP α . In the amyloidogenic pathway, APP is cleaved at the N-terminus of the A β domain by β -secretase, BACE, with the release of the soluble ectodomain fragment sAPP β . The resulting membrane-anchored C-terminal fragment is then cleaved at the C-terminus of the A β domain by γ -secretase, a multi-component complex containing the presenilins.

γ -secretase cleavage

As the final cleaving enzyme in APP proteolysis, γ -secretase is responsible for cleaving APP at the carboxy terminus (Turner *et al.*, 2003). γ -secretase is a prime contributor to the production of extracellular deposits of A β peptides 40 or 42 amino acids in length (Fossgreen *et al.*, 1998). The catalytic properties of γ -secretase plays a lead role in the proteolytic release of Notch, β -amyloid precursor protein, and other transmembrane receptors (Kimberly *et al.*, 2003). γ -secretase has been shown to endoproteolyze more than 50 type I single spanning transmembrane proteins in order to secrete short peptides in to the extracellular environment and simultaneously secrete intracellular domain into the cytosol (Wolfe *et al.*, 1999). These intracellular domains regulate cellular signaling, which indicates that γ -secretase has two roles in membrane protein metabolism; degradation, and proteolysis that influences cell signaling (Wolfe *et al.*, 1999). In Regulated Intra-membrane Proteolysis (RIP), where specific receptors in cells are cleaved into fragments and sent out to communicate with other cell compartments, γ -secretase plays a key role in determining the size of the final product (Tabaton and Tamagno, 2007).

Through post-translational modification in the endoplasmic reticulum and golgi compartments, γ -secretase forms a complex consisting of four individual proteins, presenilin, nicastrin, APH-1 (anterior pharynx-defective 1), and PEN-2 (presenilin enhancer 2) (Wang *et al.*, 2004). The roles each protein plays in γ -

secretase serve to maintain the complex and execute its designated function. Nicastrin aids in the maintenance of the protease complex and fosters protein trafficking in the complex (Takasugi *et al.*, 2003). As a glycosylated membrane protein, nicastrin is an essential protein for γ -secretase proteolytic activity and interacts with the C-terminus of APP, presenilin-1, and presenilin 2 and the N-terminal tips of substrates (Tabaton and Tamagno, 2007). The binding of N-terminal regions of substrates to nicastrin suggests that this binding site is separate from the active site of γ -secretase (Isoo *et al.*, 2007). Processing of β APP and Notch homologs in *Drosophila* is regulated by nicastrin (Tandon and Fraser, 2002). Experimental studies show that the substitution of residues on certain locations of nicastrin causes an increase in A β secretion whereas excision of these same areas prevents A β secretion (Yu *et al.*, 2004).

As a unit, Aph-1 and PEN-2 create a double membrane spanning protein and comprise the catalytic site of the complex (Takasugi *et al.*, 2003). As a membrane-spanning protein, Aph-1 forms a subcomplex with nicastrin in the early secretory pathway and regulates the transport of Aph-1/Nct to the cell surface (Turner *et al.*, 2003). PEN-2 is a hairpin-like structure that is involved in the endoproteolysis of presenilin (Tabaton and Tamagno, 2007). Mutations in any of these components may lead to irregularities in the function of the secretase. A mutation in Aph-1 or nicastrin results in a decreased expression of presenilin-1 and presenilin-2 (Isoo *et al.*, 2007). Overexpression only stabilizes γ -secretase activity (Isoo *et al.*, 2007).

Presenilin and its role in APP proteolysis

One of the primary components of γ -secretase are the presenilins. Presenilins are transmembrane proteins that span the membrane eight times and serve as the active site of protease in γ -secretase (Seidner et al., 2006). As the catalytic core of γ -secretase, presenilin is involved in intramembrane cleavage of the Notch receptor, a signaling molecule crucial for cell-fate determination during embryogenesis, as well as ErbB4, and β -amyloid precursor protein (β APP) (Takasugi *et al.*, 2003). Presenilins also undergo cleavage to form a heterodimer of N-terminal and C-terminal fragments, which are the active form of the protein (Kimberly *et al.*, 2003). The proteolytic processing of presenilin occurs within the hydrophobic region of the large cytosolic loop between transmembrane domain 6 (TM6) and transmembrane domain 7 (TM7) (Thinakaran, 1999). The presenilins are composed of two subunits, presenilin-1 (PEN-1), which is ubiquitously found in the brain and peripheral tissues, and presenilin-2 (PEN-2) which is found at low levels in the brain except in the corpus collosum, where it is high (Tandon and Fraser, 2002).

In the cells, presenilin-1, a 467 amino acid long integral membrane protein, is restricted to the endoplasmic reticulum, and although its function is unclear, may influence cellular processes such as intracellular signaling and axonal trafficking (Tandon and Fraser, 2002). Presenilin-2 is a membrane protein that binds through its first two-thirds of its first transmembrane domain (13-15) to

the transmembrane domain 4 of presenilin-1 and supports proteolytic activity in γ -secretase (Madsen *et al.*, 2007). Mutational studies have shown that length of presenilin-2 has a role in the stabilization of the presenilin complex, although its role in endoproteolytic activity is unknown (Madsen *et al.*, 2007). A mutation in presenilin-2 results in the depletion of γ -secretase activity and accumulation of a trimeric complex consisting of PS holoprotein-Nct-Aph1 (Madsen *et al.*, 2007). A missense mutation in presenilin-1 leads to the aberrant splicing out of exon 9, a region that encodes the endoproteolytic cleavage site. The presenilin-1 $\Delta E9$ variant is an active presenilin that causes A β 42 production (Wolfe *et al.*, 1999). Upon overexpression, most Presenilin-1 $\Delta E9$ is rapidly degraded similar to unprocessed wild-type presenilins; however, a small portion of this PS1 variant is stabilized in cells and forms a high molecular weight complex like the N- and C-terminal fragments, suggesting it can interact with the same limiting cellular factors as wild-type presenilins (Wolfe *et al.*, 1999). Both the presenilin-1 and presenilin-2 genes on chromosome 14 were discovered by genetic linkage analysis of a subset in Alzheimer's disease (Tandon and Fraser, 2002). A knockout of presenilin-1 only inhibits γ -secretase cleavage, whereas no alterations in a knockout of presenilin-2, may be due to compensation by the expressed presenilin-1 (Ponting *et al.*, 2001). Since presenilin is important for neuronal survival, complete knockout of presenilin-1 and presenilin-2 leads to serious consequences as seen in Alzheimer's patients (Wolfe *et al.*, 1999).

Analysis of presenilin has led to the discovery of more than 100 missense mutations and two splicing-defect mutations (Tandon and Fraser, 2002). According to Michael Wolfe and his colleagues, a mutation in highly conserved residues in presenilin-1 reduces the amount of amyloid- β and causes the accumulation of APP. Studies have indicated that mutations in presenilin appear to cause an unusual gain of function (Sisodia *et al.*, 1999). Mutant presenilins not only cause an unusual “gain of function”, which is an increase in A β 42/A β 40 production, but also results in a “loss of function” where proteolytic activity is decreased (Wolfe *et al.*, 1999). Mutations in presenilin lead to an increase in A β 42 production and decrease in A β 40 peptide production (Tandon and Fraser, 2002). In vitro A β 42 aggregates much more readily than A β 40 and as a result, triggers necrosis in muscle cells and causes degeneration (Thinakaran, 1999). In animals lacking presenilin-1 function, cleavage by γ -secretase is suppressed. Thus, the larger C-terminal APP stub accumulates in the cells (Sisodia *et al.*, 1999).

Drosophila as a Model Organism

Drosophila melanogaster, the common fruit fly, is a model organism used in the study of human diseases such as Alzheimer's, Parkinson's, and Huntington's disease. *Drosophila* is an excellent model for the study of mechanisms underlying aging and oxidative stress, and immunity found in sporadic Inclusion Body Myositis. An advantage of using the *D. melanogaster* model is that 75% of known human disease genes match fruit fly homologs (Reiter *et al.*, 2001). *D. melanogaster* has been used as a model organism to study cancer, diabetes, and drug abuse.

The versatility of *D. melanogaster* as a model organism resides in its genetic information. The *D. melanogaster* genome, curated at the flybase database (Crosby *et al.*, 2007), contains four pairs of chromosomes: an X/Y pair, and three pairs of autosomes 2, 3, and 4. The four chromosomes in the *D. melanogaster* genome allow for the manipulation of genes to produce comparative models to various diseases. The genome is ~180 Mb in size and has ~ 13,600 protein-encoding genes, which comprise ~20% of the genome (Adams *et al.*, 2000). More than 60% of the genome appears to be functional non-protein-coding DNA involved in gene expression control (Halligan and Keightley, 2006). With a sequenced genome, we are able to analyze mutations, giving us a widely accepted wildtype phenotype and genotype.

D. melanogaster has a short life cycle and, therefore allows for the study of human diseases such as neurodegenerative diseases, which typically occur at later stages in life. The developmental period for *D. melanogaster* can be manipulated with temperature (fig. 5). At 28°C (82 °F), *D. melanogaster* develops from an egg to an adult in a span of 7 days (Ashburner and Bergman, 2005). At higher temperatures (30 °C (86 °F), 11 days), developmental times increase due to heat stress. Under ideal conditions, the development time at 25 °C (77 °F) is 8.5 days, at 18 °C (64 °F) it takes 19 days and at 12 °C (54 °F) it takes over 50 days (Ashburner and Bergman, 2005). Females lay ~ 400 eggs, which are about 0.5 millimeters long, hatch after 12–15 h (at 25 °C (77 °F)). The resulting larvae grow for about 4 days (at 25 °C) while molting twice (into 2nd - and 3rd -instar larvae), at about 24 and 48 hours after eclosion. During this time, they feed on the microorganisms that decompose the fruit, as well as on the sugar of the fruit itself. Then the larvae encapsulate in the puparium and undergo a four-day-long metamorphosis (at 25 °C), after which the adults eclose (Ashburner and Bergman, 2005).

The complexity of muscle arrangement in the thorax of *Drosophila* provides for the movement of the wings, legs, and head. Muscles intrinsic for the control of locomotor appendages are direct wing and indirect wing muscles. Direct flight muscles allow for the fine control of wing position for flight while indirect wing muscles, which consists of six pairs of dorsal medial muscles, two lateral oblique dorsal muscles, three tergosternal muscles, and two tergal remotors

of coxa, control wing movement (Kozopas et al., 1998). In the thorax, the indirect flight muscles are attached to the thorax rather than the wings. In order to initiate flight, the muscles cause the thorax to deform and further cause the wings, which are extensions of the thoracic exoskeleton to move (Kozopas et al., 2008). A set of dorsal longitudinal muscles compresses the thorax from front to back, causing the dorsal surface of the thorax called the notum to bow upwards, making the wings flip upward (Kozopas et al., 1998). A set of tergosternal muscles pull the notum downwards again, causing the wings to flip upward (Kozopas et al., 2008).

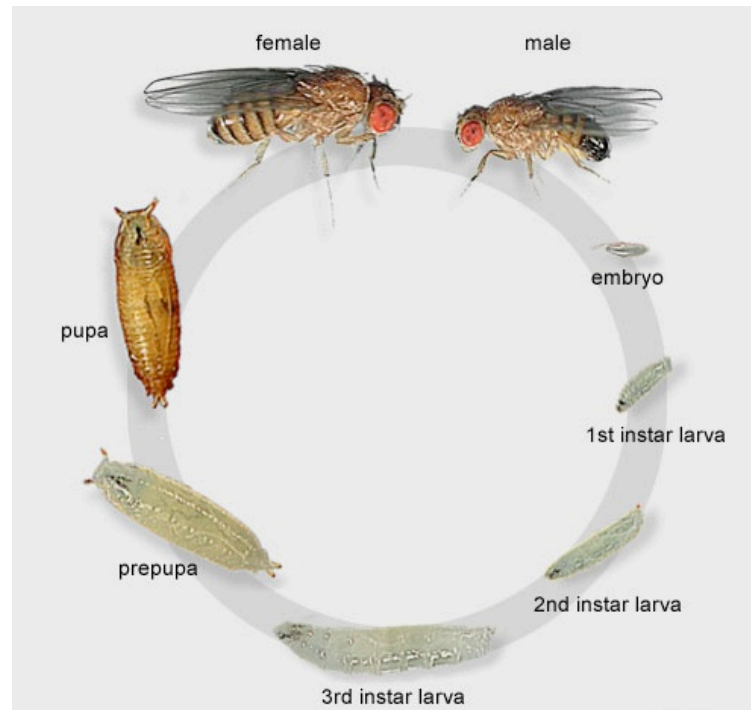


Figure 5. Life cycle of *Drosophila melanogaster*

The fertilized egg hatches after 12 – 15 hrs at 25°C. The resulting larvae grow for about 4 days (at 25°C) while molting twice (into 2nd - and 3rd -instar larvae) at about 24 and 48 hours after egg-lay. During this time, they feed on the sugar of fruits as well as on microorganisms that decompose it. At the end of the third larval instar stage, the larva crawls out of the food and ceases to move. The larvae encapsulate in the puparium and undergo a four-day-long metamorphosis (at 25°C), after which the adult flies eclose (Thompson *et al.*, 1977; Ashburner and Bergman, 2005).

Expression of APP and Presenilin in *Drosophila melanogaster*

A *D. melanogaster* model exhibiting A β -induced neurodegeneration and plaque formation provides us with a better understanding of A β peptide toxicity in Alzheimer's Disease. As is the case with presenilin, *D. melanogaster* also possesses an APP homologue that is encoded by the β -amyloid precursor protein-like (Appl) gene (Rosen *et al.* 1989). The Appl protein in *D. melanogaster* shares structural similarity to human APP and undergoes proteolytic processing but lacks homology to the short sequence of APP that gives rise to any peptide (Bonini and Fortini, 2003). Hence, the production of amyloid-like peptides and characteristics associated with the changes in brain tissue morphology and function in human Alzheimer's disease is not naturally observed in *D. melanogaster*. However, a mutation of the Appl gene results in mild behavioral defects in locomotor responses that can be reversed by introducing the flies with a functional human APP gene (Luo *et al.* 2003).

To confirm these results, studies using a mouse model have demonstrated that APP is not necessary for survival but has a role in optimal development and functioning of the nervous system, by regulating axonogenesis, dendritic arborization, or synaptic differentiation (Strooper and Annaert, 2001). In mammalian cells, during γ -secretase cleavage of APP, an amyloid peptide, and an intracellular fragment of APP are released that is involved in putative signaling activities (Cao and Sudhof, 2004).

Transgenic flies expressing wild-type and Alzheimer's disease mutant forms of APP have been generated and used to characterize the intracellular trafficking, proteolytic processing, and physiological effects of APP in *Drosophila melanogaster* (Fossgreen *et al.*, 1998). The biological properties of APP in *D. melanogaster* can be observed using overexpression strategies. Overexpressed human APP is correctly transported to synaptic terminals of neurons and postsynaptic regions of the neuromuscular junction (Yagi *et al.*, 2000), and engineered APP proteins are cleaved and secreted into the extracellular milieu (Fossgreen *et al.*, 1998). This process suggests that *D. melanogaster* is a valid model for investigating the biology of human APP. Certain features of *D. melanogaster* have been discovered from over-expression of full-length forms of APP. Wildtype or Alzheimer's disease associated mutants have been found to express a blistered wing phenotype. The blistered wing phenotype is also caused by mutations in cell adhesion molecules such as integrins, since adult fly wings develop via adhesive interactions as two epithelial cell layers that form in close apposition to one another (Brown *et al.*, 2004). The blistered wing phenotype is reminiscent of earlier findings that APP co-localizes with integrins in rat primary neurons (Storey and Cappai, 1999).

Mitochondrial defects as a phenotypic marker

Mitochondrial oxidative phosphorylation is a main source of energy in the muscles, providing the bulk adenosine triphosphate (ATP) required for most cellular functions (Hervias *et al.*, 2006). In addition to energy production, mitochondria play a crucial role in mediating amino acid biosynthesis, fatty acid oxidation, steroid metabolism, intermediate metabolic pathways, calcium homeostasis, and free radical scavenging (Kwong and Sohal, 2002). Furthermore, mitochondria are also the main source of reactive oxygen species (ROS) and central players in the intrinsic pathway of apoptotic cell death (Hervias *et al.*, 2006). Reactive oxygen species are destructive to mitochondria and are primary instigators in mitochondrial dysfunction, which ultimately leads to cell death (Kwong and Sohal, 2002). Mitochondrial dysfunction can lead to reduced ATP production, disruption of mitochondrial calcium buffering capacity, and increased generation of more reactive oxygen species. In the intermembrane space in mitochondria, certain pro-apoptotic factors such as cytochrome *c*, Smac/DIABLO, and endonuclease G are sequestered until triggered by pro-apoptotic stimuli (Kwong and Sohal, 2002). The release of cytochrome *c* in the cytosol due to pro-apoptotic stimuli leads to an interaction with the IP3 receptor (IP3R) on the endoplasmic reticulum (ER), causing an ER calcium release. This release activates caspase 9, a cysteine protease. As a result, caspase 9 activates caspase 3

and caspase 7, which are responsible for destroying the cell from within (Danial and Korsmeyer, 2004).

Mitochondrial defects and increased oxidative stress (Yang *et al.*, 2002) have been observed in patients with sIBM. Muscle fibers in these patients are cytochrome-oxidase negative, indicating mitochondrial dysfunction (Oldfors and Lindberg, 2005). Mitochondrial defects have also been noted to be present in the muscles of transgenic fly models. Subsarcolemmal aggregates of abnormal mitochondria were found in intramuscular nerves and skeletal muscle, which also showed increased mitochondrial volume and calcium levels (Hervias *et al.*, 2006). Schwartz and colleagues have found the presence of numerous swollen and damaged mitochondria in the flight muscles of transgenic flies expressing the hAPP gene (fig. 6). In addition to this anatomical data, physiological and genetic studies have implicated the accumulation of amyloid precursor protein and amyloid β to mitochondrial dysfunction (Strazielle *et al.*, 2004). The presence of APP and its proteolytic components appears to inhibit mitochondrial respiration showing the interconnectedness of these pathways (Busciglio *et al.*, 2002).

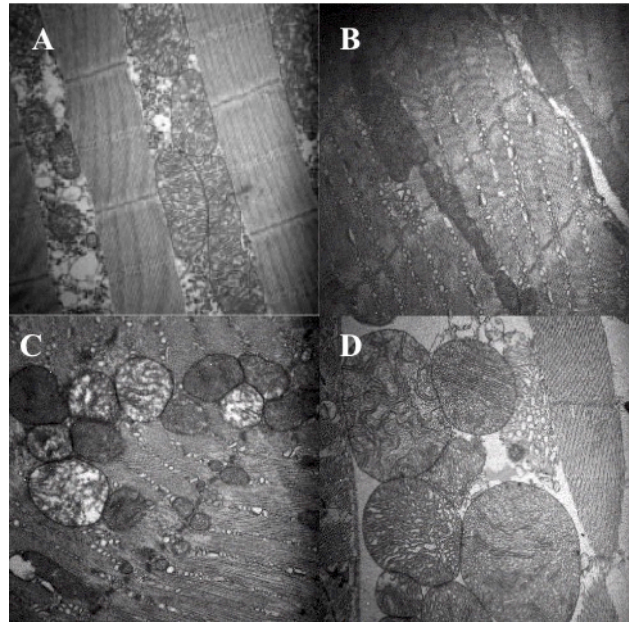


Figure 6. Transmission electron micrographs of wildtype and hAPP-expressing flight muscles

Preliminary studies showing w1118 and hAPP-expressing flies at week 1 and week 3. (A and B) micrographs are flight muscles found in wildtype at week 1 (A) and week 3 (B), respectively. (C and D) micrographs are flight muscles of hAPP-expressing flies at week 1 (C) and week 3 (D), respectively. Mitochondrial defects are noted in hAPP-expressing flies and worsen after the third week (Schwartz and Woodard, unpublished).

Aim of my research

The goal of my research is to find a protein that interacts with human APP during muscle degeneration and determine whether coexpression alleviates or exacerbates symptoms.

In order to replicate a model to understand sporadic-Inclusion Body Myositis, a team of researchers created transgenic mice that expressed the Swedish mutant hAPP in the skeletal muscles (Sugarman et al, 2002). Although symptoms are reminiscent of those found in humans, the late onset of the disease only hindered the retrieval of immediate results, making a mouse a challenging model for genetic screens. An alternative approach to challenging the slow progression of sIBM is by using *Drosophila melanogaster*. *Drosophila melanogaster* is an impressive tool for generating beneficial models of human diseases. Evidence has shown that ectopic expression of wildtype hAPP in the skeletal muscles in flies is sufficient to create a disorder that shares many phenotypic properties with human sIBM (Schwartz, unpublished). The flies have a defect in climbing and flying that is both age and activity dependent (Schwartz, unpublished). Schwartz and colleagues have shown that under transmission electron microscopy, defects in mitochondria were present. Interestingly, the presence of aggresomes was not confirmed. To analyze the sIBM disorder, we created a transgenic line containing the wildtype human APP gene under UAS

(Upstream Activating Sequence) combined with presenilin-expressing transgenes to investigate more directly the role of presenilin mutants in APP cleavage.

I hypothesize that the interaction between human APP and the expression of mutant presenilin in muscle cells may affect the structure and function of muscles in *D. melanogaster* and therefore, exacerbate the symptoms of sporadic-Inclusion Body Myositis. Alterations in presenilin function due to mutations have been found to modify γ -secretase activity in APP proteolysis. Preliminary studies have indicated that elevated cerebral levels of A β peptides from mutations in presenilin-1 cause an early and unique feature of all forms of Alzheimer's disease (Schwartz, unpublished). To confirm that an interaction between human APP and mutant presenilin exhibits phenotypic characteristics similar to patients with sporadic-Inclusion Body Myositis, transgenic flies were subjected to climbing and flight assays. Results will compare flies coexpressing hAPP and presenilin to wildtype and hAPP flies. The *D. melanogaster* model will allow us to generate evidence that IBM-like disorders are not only influenced by genetic factors, but also by environmental factors that aggravate symptoms affected by muscle degeneration. Defects in muscle mitochondria have been observed to precede the onset of behavioral symptoms, which suggest it to be a useful tool for understanding the pathogenesis of IBM-like disorders and for identifying genes and small molecules that can delay the onset or severity of symptoms. The significance of this work will to allow us to identify candidate targets for therapeutic intervention for the treatment of sIBM.

MATERIALS AND METHODS

UAS-Gal4 System

To model amyloid plaque pathology and neurodegeneration in *D. melanogaster*, transgenic flies were engineered to coexpress hAPP and presenilin, presenilin alone, and hAPP alone. The UAS/Gal4 system was used for target gene expression in the muscle cells of these flies. In *Drosophila*, combinatorial ectopic expression of APP and presenilin leads to the formation of A β plaques in the neurons (Schwartz, unpublished). The transgenic fly line that was used encodes the human APP cDNA under the control of the Gal4 transcription factor (Luo *et al.*, 2003). This transgene is inserted on the second chromosome. These flies were crossed with a line containing a Dmef-Gal4 insert on the third chromosome, which drives the expression of the Gal4 transcription factor in muscle cells (Lilly *et al.*, 1994). UAS was located adjacent to the hAPP gene on chromosome 3. Gal 4 encodes a transcription factor protein that drives expression of any genes adjacent to the UAS promoter. Gal 4 was inserted next to the Dmef promoter. Dmef specifies the expression of adjacent genes only in muscle cells. Through this system, hAPP was specifically expressed in the muscle cells of *Drosophila*. A stock line (*UAS-humanAPP;Dmef-Gal4/Cyo-TM6*) was created using a second and third fused chromosome balancer (*W/+; Sp/Cyo-TM6*) (Wing *et al.*, 2002).

This line was used to screen for possible target genes that act as modifiers of APP function in IBM disease.

Crosses to Generate Experimental Genotypes

In order to prepare the flies for the climbing and flight assay, each stock line was reared in bottles. The bottles containing each stock line were incubated for 8 hours at 25°C or for 18 hours at 18°C for daily collection of virgin flies. Virgin females were collected from *UAS-PsnE280.A2/TM3, sb* and *UAS-Psn L237.2A/TM3, sb* periodically in standard vials until there were enough flies to cross. Males were collected from *UAS-hAPP; Dmef-Gal4/Cyo-TM6* and *Dmef-Gal4* to make the cross.

Four genotypes were evaluated using both climbing and flight assays (fig.7). Each stock was bred in standard vials and observed for three to five consecutive days for eclosion. Once larvae were present, the parents were transferred into new vials to generate more F₁ progeny. Larvae were divided into two different vials; siliconized and standard. In order to prepare siliconized vials, standard plastic vials were submerged in Armorall Autoglass cleaner, and left to dry overnight. The vials were washed with water the next morning and dried overnight or over two nights and stored. Newly eclosed adults were collected and placed in their respective environments (standard/siliconized) and labeled with the date of eclosion. About 20-30 flies of each genotype were collected at each

eclosion date. These eclosed adults were left in their respective vials for five days and then isolated and anesthetized 48 hours before an assay. Flies were isolated to select appropriate genotypes by using phenotypic balancers to distinguish between the flies. Curly wing (CyO) and stubble bristle (TM3) flies were discarded while flies that exhibited wildtype phenotype were selected. The selected flies were then placed in their respective environments for two days and a climbing/flight assay was conducted on the second day.

$$\begin{array}{ccc} \text{♂} & \frac{UAS-hAPP ; Dmef-Gal 4}{CyO - TM6} & \times \frac{+ ; UAS-Psn L^{237.2A}}{+ TM3, Sb} \text{♀} \end{array}$$



$$\frac{UAS-hAPP ; Dmef-Gal 4}{+ UAS-PsnL^{237.2A}}$$

$$\begin{array}{ccc} \text{♂} & \frac{UAS-hAPP ; Dmef-Gal 4}{CyO - TM6} & \times \frac{+ ; UAS-Psn E^{280.A2}}{+ TM3, Sb} \text{♀} \end{array}$$



$$\frac{UAS-hAPP ; Dmef-Gal 4}{+ UAS-PsnE^{280.A2}}$$

$$\text{♂ } \frac{UAS-hAPP; Dmef-Gal 4}{CyO - TM6} \times \frac{UAS-hAPP; Dmef-Gal 4}{CyO - TM6} \text{ ♀}$$



$$\frac{UAS-hAPP}{UAS-hAPP} ; \frac{Dmef-Gal 4}{Dmef-Gal 4}$$

$$\text{♂ } \frac{+ ; Dmef-Gal 4}{+ Dmef-Gal 4} \times \frac{+ ; UAS-Psn L^{237.2A}}{+ TM3, Sb} \text{ ♀}$$



$$\frac{+ ; Dmef-Gal 4}{+ UAS-PsnL^{237.2A}}$$

$$\text{♂ } \frac{+ ; Dmef-Gal 4}{+ Dmef-Gal 4} \times \frac{+ ; UAS-Psn E^{280.A2}}{+ TM3, Sb} \text{ ♀}$$



$$\frac{+ ; Dmef-Gal 4}{+ UAS-PsnE^{280.A2}}$$

Figure 7. Stock lines using the UAS and Dmef-Gal4 system to express the appropriate genotypes in muscle cells

Used to test the affect of hAPP on behavior. All flies showing curly wing (CyO), stubble bristle (TM3) were discarded. Those flies that did not show the specific phenotype of the balancers were saved in specific vials and the date of eclosion was noted.

Climbing Assay

The newly eclosed adults were placed at 25°C for five days for selection. On the fifth day, flies were anesthetized 48 hours prior to the climbing assay. Flies expressing the curly wing (CyO), stubble bristle (TM3) were discarded while flies expressing a wildtype phenotype were saved for the assays. On the seventh day climbing assays were conducted. Each vial of flies was tested separately. The flies were tapped into a 50ml plastic graduated cylinder and given one minute to recover. The graduated cylinder was tapped again to restart the climb. Flies that reached the above the 30ml mark within 15 seconds were counted and recorded as a successful climb. The test was repeated for each vial three times and the average percentage climbing for each test group was determined and compared to the climbing behavior of age-matched controls. The climbing assay was performed weekly to test their ability to climb until the fifth week and the average percentage climbing for each test group was determined and compared to the climbing behavior of age-matched controls. Each vial was replaced weekly so that larvae produced by the flies could not mix with the selected flies. The vials were preserved in a 25°C refrigerator throughout the five weeks.

Flight Assays

After four weeks of climbing assays a flight assay was performed. A 500 mL glass graduated cylinder was coated with mineral oil. The flies were tapped into the graduated cylinder and evaluated on the basis of where they landed. Flies were counted at each increment of 100mL where they landed and recorded. The test was done once for each vial and the graduated cylinder was cleaned out for each test by sifting the mineral oil from the flies. Mineral oil was replaced for each flight assay.

Transmission Electron Microscopy

Preparation for the transmission electron microscope involved the fixation of *Drosophila* muscle cells. Three crosses w^{1118} , $PsnL^{237}$ alone, and $hAPPxPsnL^{237}$ were collected during the first and third week and prepared for microscopy. To prepare the flies for TEM a roughly rectangular portion of the cuticle on the dorsal side of the thorax was removed to expose the muscle and allow penetration of solutions and resin. Five flies from each cross were anesthetized and placed in a vial on ice. Using a pipette, the dissection was performed in fixative (2.5% glutaraldehyde, 2.5% formaldehyde in 0.1M sodium cacodylate buffer, pH 7.3) and fixation was continued at 4⁰ C overnight. Flies were rinsed in 0.1M sodium cacodylate, pH7.3 for 1 hour (6 x 10 minutes each) and post-fixed in 1% osmium

tetroxide in 0.1M sodium cacodylate buffer, pH 7.3 for 1 hour at room temperature. After rinsing in 0.1M sodium cacodylate buffer the flies were *en bloc* stained with 1% uranyl acetate for 30 minutes in the dark. They were then dehydrated in 30, 50, 70, 90, 95% ethanol for 15 – 30 minutes each and 3 x 100% ethanol. The flies were slowly infiltrated with Spurr's resin (1 – 2 hours each concentration and overnight in 100% Spurr's) and embedded in both flat pans and flat rectangular molds. Polymerization was at 60⁰C for 24 hours. Sections (60 – 70 nm) were taken with a Reichert Ultracut ultramicrotome, post-stained with 1% uranyl acetate and Reynold's lead citrate and examined on a Philips CM100 transmission electron microscope.

RESULTS

Climbing Assays

In order to evaluate the effect that coexpression of human APP and mutant presenilin has on behavior and activity, the flies were subjected to climbing assays. Flies coexpressing hAPP and presenilin were compared to w^{1118} , flies expressing human APP (hAPP), and flies expressing mutant presenilin. Two alleles in presenilin, $PsnL^{237}$ and $PsnE^{280}$, were observed under activity conditions over a period of four weeks. No statistical data is shown of the assays since this is a preliminary study. More experiments must be done to gain accurate statistical results.

PsnE280 lines

In the $PsnE^{280}$ climbing assays to evaluate, the w^{1118} control flies show a slight decrease in successful climbing activity over age. Flies that passed the 30mL mark within 15 seconds were recorded as a successful climb. The difference in success between week 1 and 4 is approximately 42.6% for the standard and 37.1% for the siliconized-vial flies (fig.8). The wildtype flies displayed no extraordinary change in climb despite of living environment.

Flies expressing *hAPP* alone displayed a decreasing trend in climbing ability over a period of four weeks. Standard-vial flies displayed a difference in success between week 1 and 4 of approximately 55.4% (fig.9). Siliconized-vial

flies displayed a difference in success between week 1 and 4 of approximately 61.1%. Standard-vial flies began the first week with an 88% successful climb and siliconized-vial flies began with a 77.1% successful climb. The standard and siliconized-vial flies seem to drop dramatically in climb at three weeks. During the fourth week, standard-vial flies do not exhibit any dramatic change in successful climb. Conversely, the siliconized-vial flies dramatically dropped in successful climb after three weeks to a lower percent in successful climb in the fourth week. Overall, siliconized-vial flies had a lower percent in successful climb than in the standard-vial flies.

Flies expressing *PsnE*²⁸⁰ displayed a decreasing trend in climbing ability over a period of four weeks. Standard-vial flies displayed a difference in success between week 1 and 4 of approximately 66.9% (fig.10). Siliconized-vial flies displayed a difference in success between week 1 and 4 of approximately 41%. Standard-vial flies began the first week with a 95% successful climb and siliconized-vial flies began with an 84% successful climb. Standard-vial flies show a dramatic drop in successful climb after two weeks and maintain the same percent of successful climb up to the fourth week. The siliconized-vial flies increase in climbing ability at three weeks and then slightly decrease in climbing ability after the fourth week. Siliconized-vial flies demonstrate a higher successful climb than the standard-vial flies.

Flies coexpressing *hAPP x PsnE*²⁸⁰ displayed a decreasing trend in climbing ability over a period of four weeks. Standard-vial flies displayed a

difference in success between week 1 and 4 of approximately 46% (fig. 11). Siliconized-vial flies displayed a difference in success between week 1 and 4 of approximately 39.4%. Standard-vial flies began in the first week with a 96% successful climb while siliconized-vial flies began with 87.2% successful climb. Standard-vial flies demonstrated no dramatic changes in climbing ability. After three weeks, climbing ability began to decrease. The siliconized-vial flies, displayed a decrease in climbing ability after two weeks but began to increase in climbing ability after three weeks. The siliconized vial flies seem to decrease at a similar rate as the standard vial flies but maintained a lower percent of successful climb.

The four genotypes were compared to each other on a graph to assess any relationships in account of climbing ability. The general trend in all the standard lines is a decrease in climbing ability with age (fig. 12). Among all the climbing assays, the w^{1118} control showed the highest percent of successful climb at week one with 97.8% compared to all the other lines. The lowest, $hAPP$, began at week one with 88%. $PsnE^{280}$ began to decrease at a similar rate as the w^{1118} but dramatically dropped at three weeks and ends with a lower percentage of successful climb than $hAPP$. The $hAPP \times PsnE^{280}$ line showed a small drop in climbing ability after the third week but showed a higher percent in climbing ability compared to the $hAPP$ and $PsnE^{280}$ lines. While the $hAPP$ line showed its greatest decrease in ability between the second and third week, the $PsnE^{280}$ line showed its decrease between the third and fourth week.

The general trend in all the siliconized lines is a decrease in climbing ability with age (fig. 13). Among all the climbing assays, the w^{1118} control showed the highest percent of successful climb during the first week with 90.1% compared to all the other lines. The lowest, $hAPP$, began at the first week with 77.1%. The $PsnE^{280}$ and $hAPP \times PsnE^{280}$ lines demonstrated a fluctuation in climbing ability throughout the four weeks. The $PsnE^{280}$ line began at a lower percentage, maintained a gradual decrease, and then dropped lower than the flies coexpressing $hAPP \times PsnE^{280}$. The $hAPP \times PsnE^{280}$ line showed an exact trend in climbing ability but maintained showed a greater climbing ability compared to the $hAPP$ and $PsnE^{280}$ lines. While the $hAPP \times PsnE^{280}$ showed its greatest decrease in ability between the second and third week, $PsnE^{280}$ alone showed its decrease between the third and fourth week.

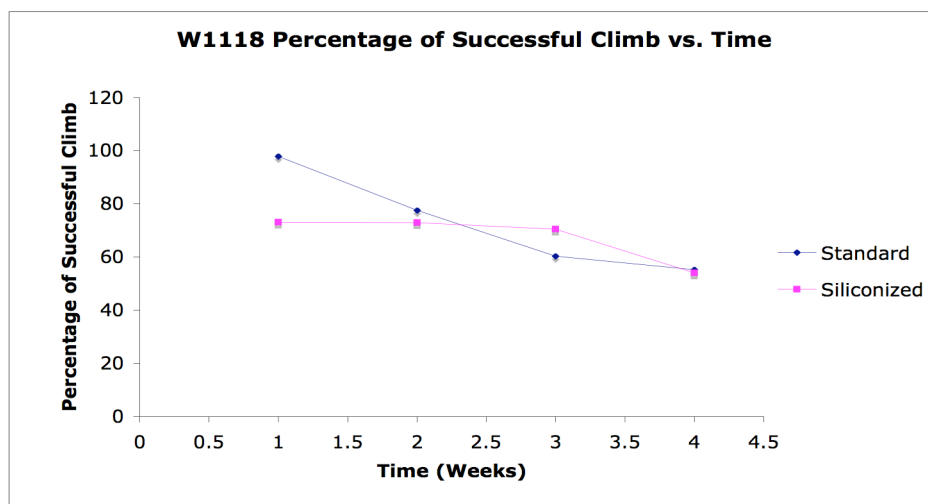


Figure 8. The w^{1118} control standard and siliconized-vial climbing assay results

Standard-vial flies display a better climbing ability than the siliconized vial flies. Siliconized-vial flies display a drop in climbing ability at 3 weeks

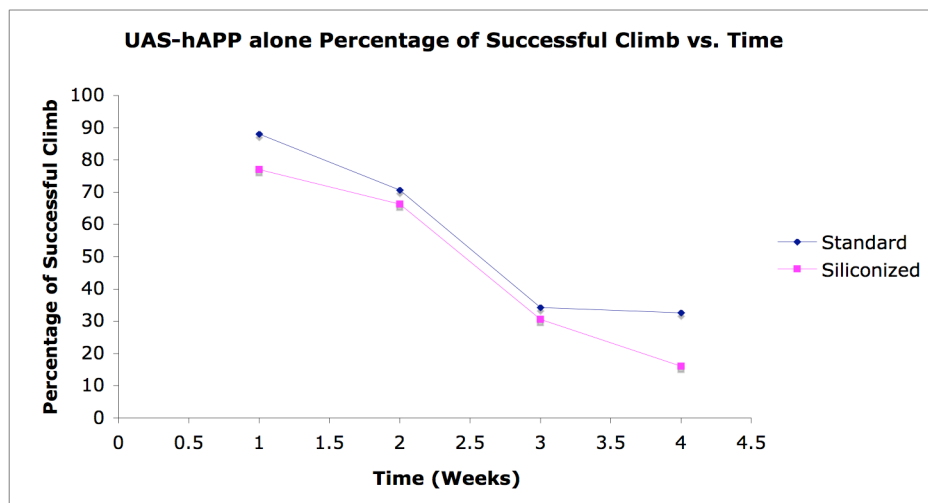


Figure 9. $hAPP$ -expressing standard and siliconized-vial climbing assay results

Standard-vial flies display a better climbing ability than the siliconized vial flies. Siliconized-vial flies display a drop in climbing ability at 3 weeks

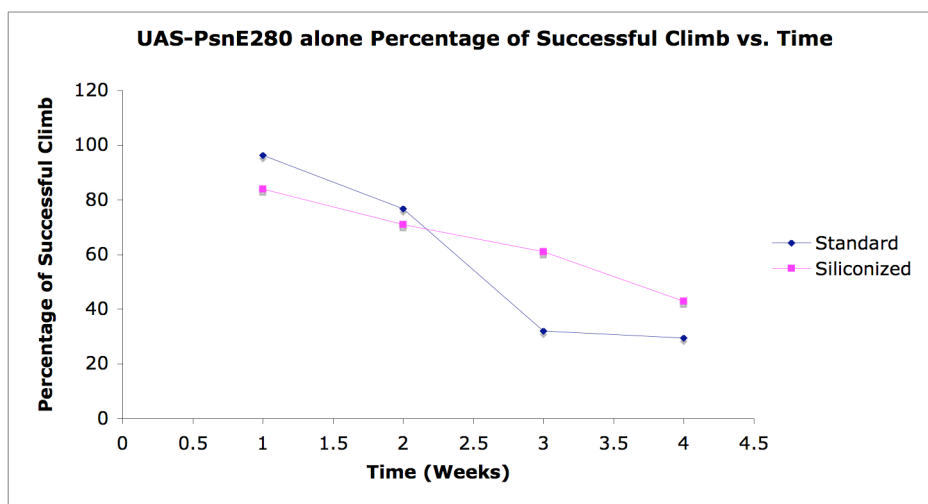


Figure 10. *PsnE²⁸⁰* standard and siliconized-vial climbing assay results
 Standard-vial flies display a better climbing ability from week 1 to week 2. Siliconized display a higher climbing ability 3 weeks

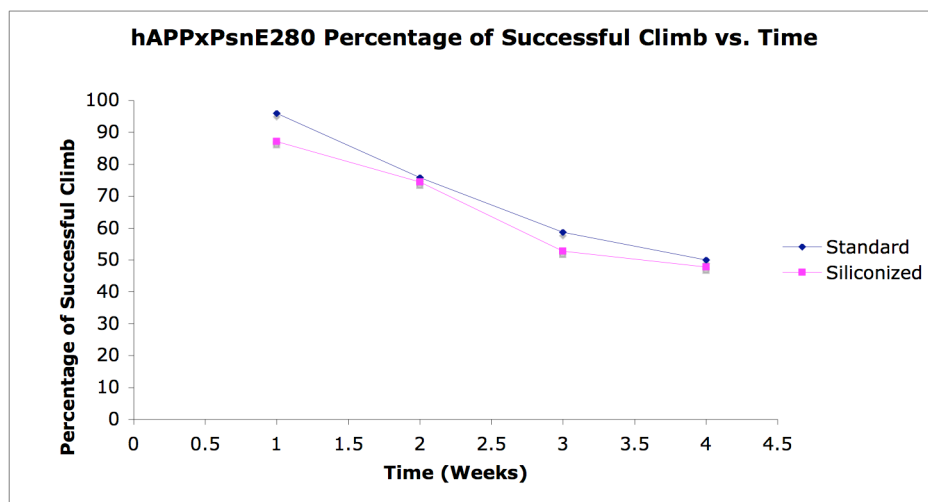


Figure 11. Flies coexpressing *hAPPxPsnE²⁸⁰* standard and siliconized-vial climbing assay results
 Standard-vial flies display a better climbing ability than the siliconized vial flies. At 4 weeks, the standard and siliconized-vial flies display a close climbing ability

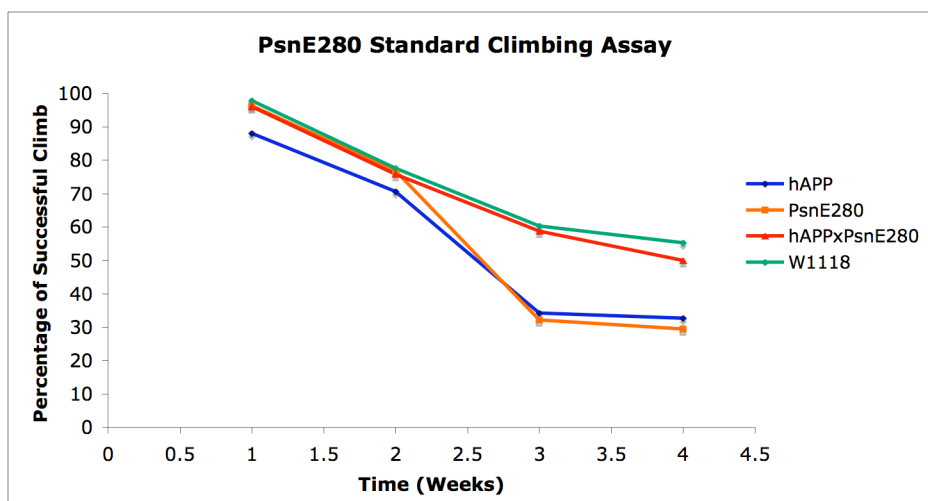


Figure 12. Standard climbing assay of $PsnE^{280}$, $hAPPxPsnE^{280}$, $hAPP$ and w^{1118}

A general trend in all the genotypes is a decrease in climbing ability with age. The w^{1118} control displays the highest percent of successful climb while the lowest percent of successful climb is in $hAPP$ -expressing flies from week 1 to week 2. $PsnE^{280}$ dramatically drops at week 3 and flies coexpressing $hAPPxPsnE^{280}$ gradually decreases.

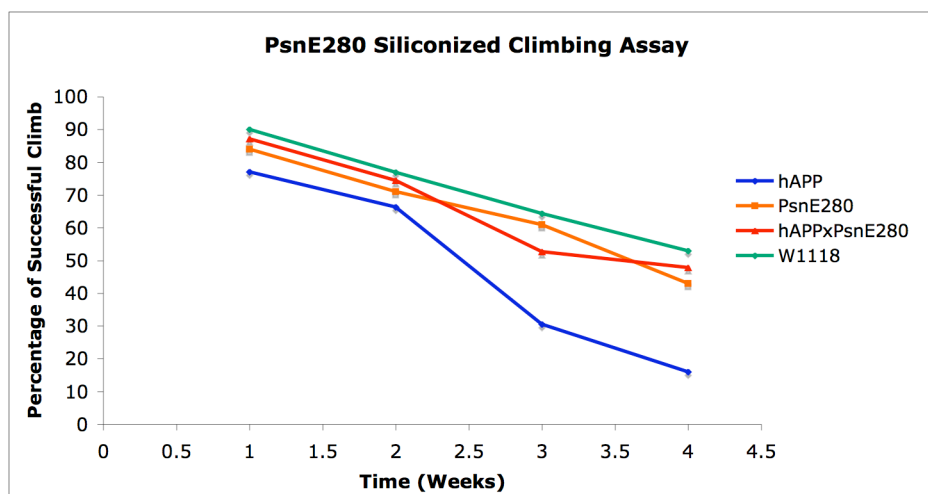


Figure 13. Siliconized climbing assay of $PsnE^{280}$, $hAPPxPsnE^{280}$, $hAPP$ and w^{1118}

A general trend in all the genotypes is a decrease in climbing ability with age. The w^{1118} control displays the highest percent of successful climb while the lowest percent of successful climb is in $hAPP$ -expressing flies. Fluctuation in climbing ability occurs at three weeks for $PsnE^{280}$ and flies coexpressing $hAPPxPsnE^{280}$

PsnL237 lines

The *PsnL²³⁷* climbing assay was conducted at a separate time point with new age-related *w¹¹¹⁸* controls and *hAPP*-expressing flies. Standard-vial *w¹¹¹⁸* flies displayed a difference in success between week 1 and 4 of approximately 42.6%. Siliconized-vial flies displayed a difference in success between week 1 and 4 of approximately 33.6% (fig. 14). The *w¹¹¹⁸* flies displayed no extraordinary change in climb despite living conditions.

Flies expressing *hAPP* displayed an expected decreasing trend in climbing ability over a period of four weeks. Standard-vial flies displayed a difference in success between week 1 and 4 of approximately 56.1%. Siliconized-vial flies displayed a difference in success between week 1 and 4 of approximately 47.7% (fig. 15). Standard-vial flies began in the first week with an 83.6% successful climb while siliconized-vial flies begin with an 84.4% successful climb. Both standard-vial and siliconized-vial flies dramatically drop in climbing ability after three weeks. During the fourth week, standard-vial flies displayed a slight decrease in climbing ability. On the contrary, the siliconized-vial flies increased in climbing ability after four weeks. Overall, standard-vial flies scored a lower climbing ability than the siliconized-vial flies.

Flies expressing *PsnL²³⁷* displayed a decreasing trend in climbing ability over a period of four weeks. Standard-vial flies displayed a difference in success between week 1 and 4 of approximately 39.9%. Siliconized-vial flies displayed a difference in successful climb between week 1 and 4 of approximately 40.8%

(fig.16). Standard-vial flies began the first week with an 89.9% successful climb while siliconized-vial flies began with an 88% successful climb. After the second week, standard-vial flies dramatically dropped in climbing ability but maintained climbing ability until the fourth week. Siliconized-vial flies decreased in climbing ability during the second week, increased in climbing ability during the third week, and ultimately decreased in climbing ability during the fourth week. During the fourth week, siliconized-vial flies had a lower success in climb than the standard-vial flies.

Flies coexpressing *hAPP x PsnL²³⁷* displayed a decreasing trend in climbing ability over a period of four weeks. Standard-vial flies displayed a difference in success between week 1 and 4 of approximately 46.9% (fig.17). Siliconized-vial flies displayed a difference in success between week 1 and 4 of approximately 41.1%. Standard-vial flies began in the first week with a 95.1% successful climb while siliconized-vial flies began with an 89.8% successful climb. The standard-vial flies displayed a gradual decrease over time. At four weeks, the standard-vial flies increased in climbing ability. The siliconized-vial flies decrease in climbing ability at two weeks, increases in climbing ability at three weeks, and ultimately decreases in climbing ability at the fourth week similar to the *PsnL²³⁷* line.

The four genotypes were compared to each other on a graph to evaluate the percent of successful climb. The general trend in all the standard-vial lines is a decrease in climbing ability with age (fig. 18). Among all the climbing assays,

w^{1118} control showed the highest percent of successful climb at week 1 with 97.8% compared to all the other lines. The lowest, *hAPP*, began in the first week with 83.6%. The *hAPP x PsnL²³⁷* line displayed a gradual decrease in climbing ability whereas the *PsnL²³⁷* line dropped dramatically in climbing ability from the first week into the second week. During the third week, *PsnL²³⁷* maintained a high successful climb while *hAPPxPsnL²³⁷* had a lower percent of successful climb. In the fourth week, the *hAPPxPsnL²³⁷* and *PsnL²³⁷* lines had close percentages in climbing ability. The *hAPP* line displayed the lowest percent of successful climb in all weeks.

The general trend in all the siliconized-vial lines is a decrease in climbing ability with age (fig. 19). Among all the climbing assays, w^{1118} showed the highest percent of successful climb at week 1 with 93.7% compared to all the other lines. The lowest, *hAPP*, began at week 1 with 84.4%. *PsnL²³⁷* and *hAPPxPsnL²³⁷* followed a decrease in climbing ability during the second week, an increase in climbing ability during the third week, and ultimately a decrease in climbing ability during the fourth week. Throughout the climbing assay, *hAPP* had the lowest successful climb throughout all four weeks.

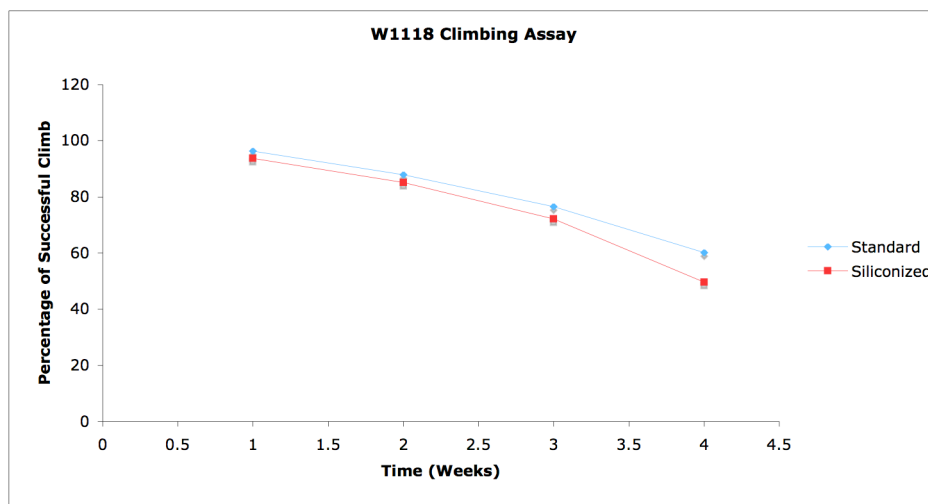


Figure 14. The w^{1118} standard and siliconized-vial climbing assay results
The standard-vial flies display a higher climbing ability than the siliconized-vial flies.

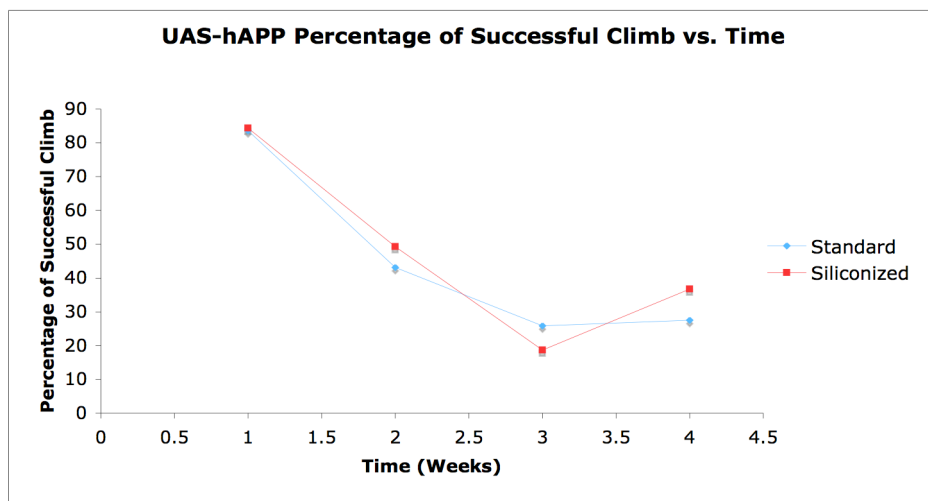


Figure 15. $hAPP$ -expressing standard and siliconized-vial climbing assay results
Siliconized-vial flies display a better climbing ability than standard vial flies for two weeks. At week 3, siliconized-vial flies display a drop in climbing ability

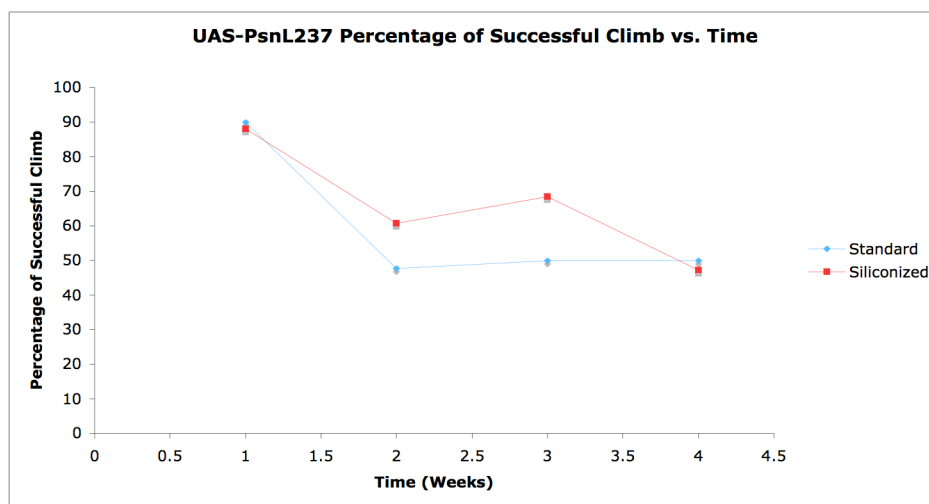


Figure 16. *PsnL*²³⁷ standard and siliconized-vial climbing assay results
 Siliconized-vial flies display a higher climbing ability than standard vial flies. Standard-vial flies show a gradual decrease up to week 2 and then gradually increases in climbing ability

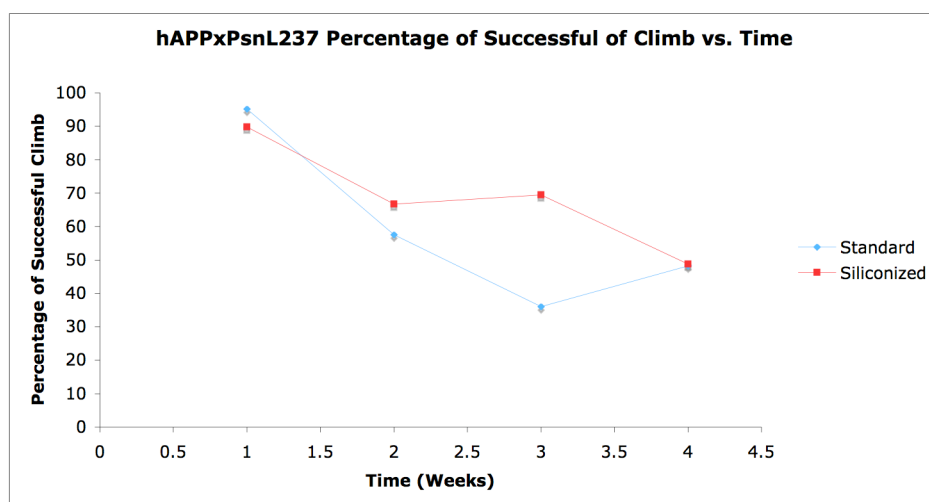


Figure 17. Flies coexpressing *hAPPxPsnL*²³⁷ standard and siliconized-vial climbing assay results
 Siliconized-vial flies display a higher climbing ability than standard vial flies. Standard-vial flies show a gradual decrease in climbing ability

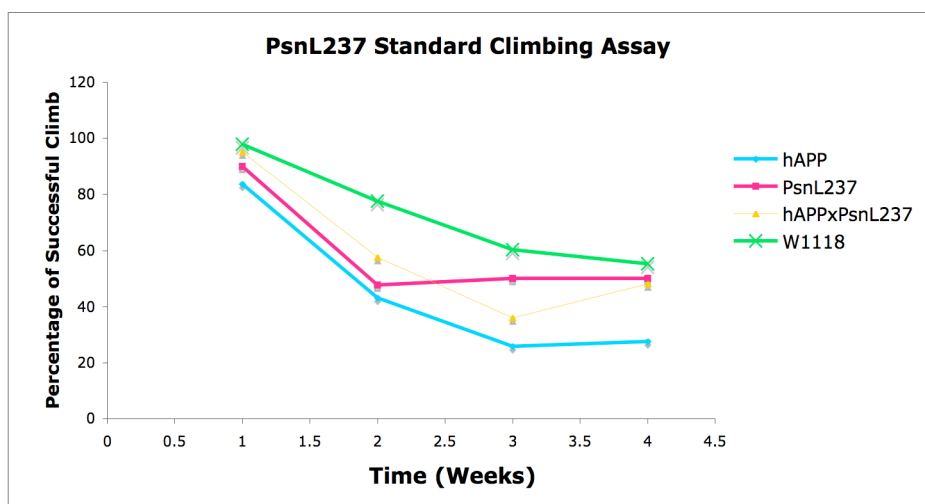


Figure 18. Standard climbing assay of $PsnL^{237}$, $hAPPxPsnL^{237}$, $hAPP$ and w^{1118}

A general trend in all the genotypes is a decrease in climbing ability with age. The w^{1118} control displays the highest percent of successful climb while the lowest percent of successful climb is in $hAPP$ -expressing flies.

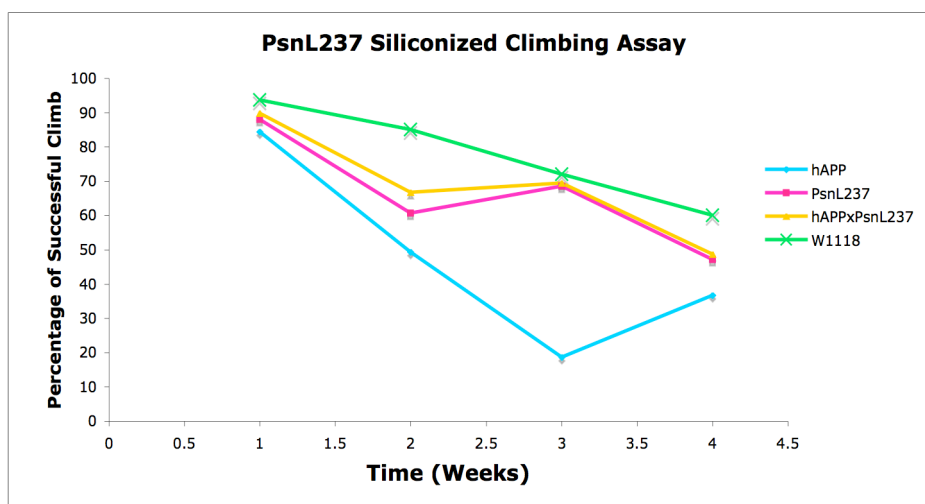


Figure 19. Siliconized climbing assay of $PsnL^{237}$, $hAPPxPsnL^{237}$, $hAPP$ and w^{1118}

A general trend in all the genotypes is a decrease in climbing ability with age. The w^{1118} control displays the highest percent of successful climb while the lowest percent of successful climb is in $hAPP$ -expressing flies. $PsnL^{237}$ and flies coexpressing $hAPPxPsnL^{237}$ follow a zig-zag trend.

Flight Assays

The flight assays were conducted to determine whether the use of flight muscles correlated with muscle degeneration in the legs. During the fifth week, all the lines were subjected to flight assays and compared to each other.

PsnE280 lines

The flight assay for w^{1118} , displayed a high percentage of flies that landed between the 300 - (>500)mL mark compared to the percentage of flies that landed between 0-300mL (fig. 20). About 70.7% of standard-vial flies landed at 300mL and above and 23.4% landed below 300mL. In the siliconized-vial flight assay, about 74.7% landed at 300mL and above and 25.3% of flies landed at 300mL and below. The majority of standard-vial and siliconized-vial flies landed between 400-500mL. The lowest percent of flies for the standard-vial flies landed between 1-100mL while the lowest percent of siliconized-vial flies landed at 200-300mL.

In flies expressing *hAPP*, a high percent of flies landed at the 300mL mark and above (fig. 21). Among standard-vial flies, 65.3% of the flies landed at 300mL and above and 34.7% of the flies landed below 300mL. About 74.2% of siliconized-vial flies landed at 300mL and above, while 25.8% landed below 300mL. The highest percentage of standard-vial and siliconized-vial flies landed between 400-500mL. Both the standard-vial flies and siliconized-vial flies had the lowest percent of flies between the 100-200mL mark.

Flies expressing *PsnE²⁸⁰* displayed a high percent of flies that landed at 300mL and above (fig. 22). The standard-vial flies showed a percent of 51.2% above the 300mL mark and 48.8% below the 300mL mark. Siliconized-vial flies had about 56.7% of flies that landed above 300mL and 43.3% of flies below the 300mL mark. In the standard-vial flight assay, the highest percent of flies landed between 400-500mL while the lowest percent of flies landed between 100-200mL. Siliconized-vial flies had the highest percent of flies between 0-100mL and the lowest percent of flies between 100-200mL.

Flies coexpressing *hAPP x PsnE²⁸⁰* displayed a high percentage of flies at 300mL and above (fig. 23). Among the standard-vial flies, a high percentage landed between 300mL and above with 62.7%, while a low percent of flies, landed below 300mL with 37.3%. The siliconized-vial flies showed a high percentage of flies at 300mL and above with 65.3% while 34.7% of flies landed below the 300mL mark. Standard-vial flies landed primarily at 500mL and above and a low percent of standard-vial flies landed between 100-200mL. Siliconized-vial flies showed a high percentage of flies between 300-400mL while the lowest percent of siliconized-vial flies landed between 100-200mL.

The standard-vial flight assay data of the *PsnE²⁸⁰* lines were compared on a graph (fig. 24). At 0-100mL, the *w¹¹⁸* control displayed the lowest percent of flies that landed compared to flies expressing *hAPP* and *hAPPxPsnE²⁸⁰*. Flies expressing *PsnE²⁸⁰* had the highest percent of flies that landed. At 100-200mL, the lowest percent of flies that landed were flies expressing *hAPP* while flies

coexpressing *hAPPxPsnE²⁸⁰* had the highest percent of flies that landed. At 200-300mL, the *w¹¹¹⁸* control displayed the lowest percent of flies that landed while the highest percent of flies that landed were flies expressing *hAPP*. At 300-400mL, flies expressing *PsnE²⁸⁰* displayed the lowest percent of flies that landed while the *w¹¹¹⁸* control displayed the highest percent of flies that landed. At 400-500mL, flies coexpressing *hAPPxPsnE²⁸⁰* displayed the lowest percent of flies that landed compared to the highest percent of flies expressing *hAPP* that landed. At 500mL and above, flies expressing *PsnE²⁸⁰* displayed the lowest percent of flies that landed while the highest percent of flies that landed were flies coexpressing *hAPPxPsnE²⁸⁰*.

The siliconized-vial flight assay data of the *PsnE²⁸⁰* lines were compared on a graph (fig. 25). At 0-100mL, the *w¹¹¹⁸* control had the lowest percent of flies whereas flies expressing *PsnE²⁸⁰* displayed the highest percent of flies that landed. At 100-200mL and 200-300mL, flies expressing *hAPP* had the lowest percent of flies that landed whereas flies coexpressing *hAPPxPsnE²⁸⁰* displayed the highest percent of flies that landed. At 300-400mL, flies expressing *PsnE²⁸⁰* had the lowest percent of flies whereas flies expressing *hAPP* had the highest percent of flies that landed. At 400-500mL, flies coexpressing *hAPPxPsnE²⁸⁰* display the lowest percent of flies that landed whereas the *w¹¹¹⁸* control has the highest percent of flies that landed. At 500mL and above, the *w¹¹¹⁸* control displayed the lowest percent of flies whereas flies coexpressing *hAPPxPsnE²⁸⁰* displayed the highest percent of flies that landed.

Overall, the standard-vial and siliconized-vial flight assays displayed similarities and differences between genotypes. At 0-100mL, in the standard-vial and siliconized-vial flight assays, the w^{1118} control displayed the lowest percent of flies compared to the other flies and flies expressing $PsnE^{280}$ displayed the highest percent of flies that landed. Similarities were also displayed at 100-200mL, where flies expressing $hAPP$ showed the lowest percent of flies and flies coexpressing $hAPPxPsnE^{280}$ displayed the highest percent of flies in both standard-vial and siliconized-vial flies. Results varied after 200ml and no patterns were noted.

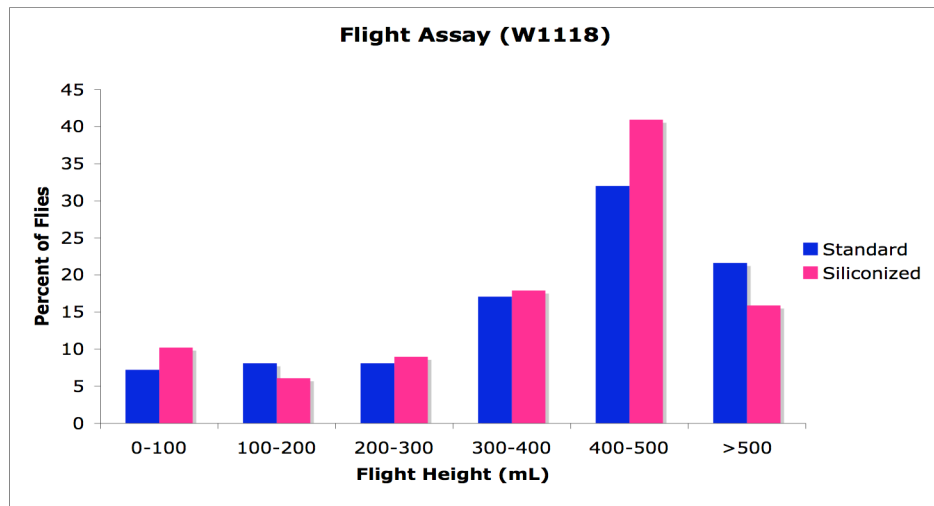


Figure 20. Flight Assay Result of the w^{1118} controls in Standard and Siliconized Vials

The greatest percentage of standard and siliconized samples scored at 400-500mL

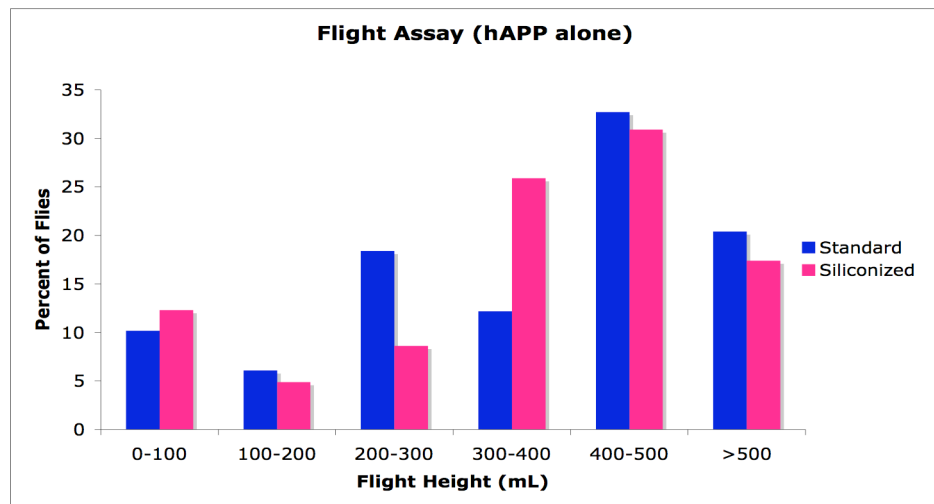


Figure 21. Flight Assay Result of $hAPP$ – expressing flies in Standard and Siliconized Vials

The greatest percentage of standard and siliconized samples scored at 400-500mL

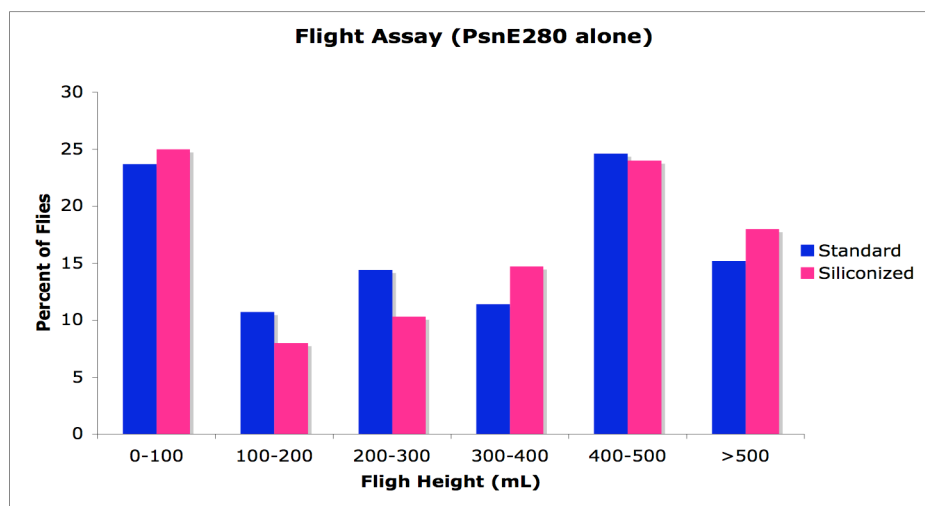


Figure 22. Flight Assay Result of *PsnE*²⁸⁰ in Standard and Siliconized Vials
 The greatest percentage of siliconized samples scored at 0-100mL, and standard samples scored at 400-500 mL.

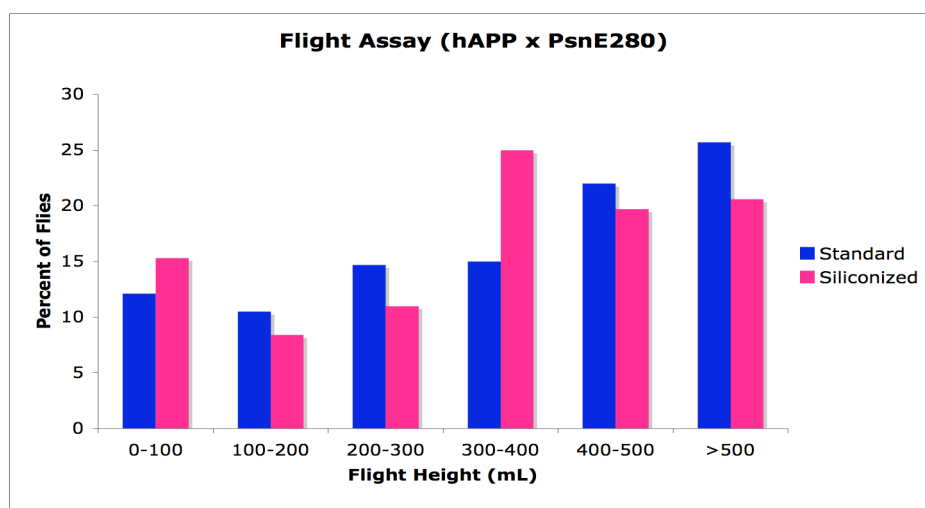


Figure 23. Flight Assay Result of *hAPPxPsnE*²⁸⁰ in Standard and Siliconized Vials
 The greatest percentage of siliconized samples scored at 300-400mL, and standard samples scored at >500 mL.

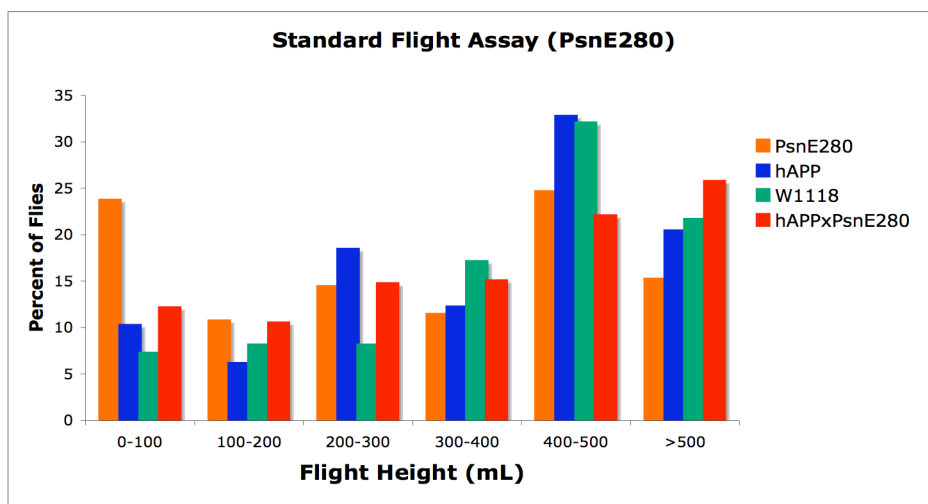


Figure 24. Standard flight assay of $PsnE^{280}$, $hAPPxPsnE^{280}$, $hAPP$ and w^{1118}
 The majority of flies landed at 300mL and above. The w^{1118} control shows a gradual increase in percent of flies that landed from 0mL being the least and 500mL the most. All the other genotypes showed no particular pattern.

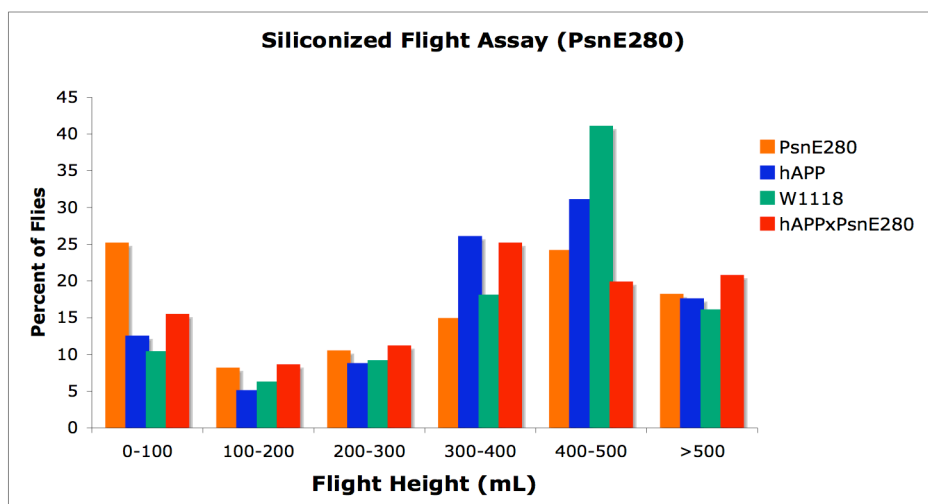


Figure 25. Siliconized flight assay of $PsnE^{280}$, $hAPPxPsnE^{280}$, $hAPP$ and w^{1118}
 The majority of flies landed at 300mL and above. The w^{1118} control shows a gradual increase in percent of flies that landed from 100mL being the least and 500mL the most. All the other genotypes showed no particular pattern.

PsnL237 lines

The flight assay for *W¹¹¹⁸*, displayed a high percentage of flies that landed between that 300-(>500)mL mark compared to the percentage of flies that landed between 0-300mL. About 71.7% of standard-vial flies landed at 300mL and above and 28.3% of flies landed below 300mL. In the siliconized-vial flies flight assay, 67.2% of flies landed at 300mL and above while 32.8% of flies landed at 300mL and below (fig. 26). The highest percent of flies for both the standard-vial and siliconized-vial flies landed between 400-500mL. The lowest percent of flies for the standard-vial flies landed between 1-100mL whereas in the siliconized-vial flies, the lowest percent landed at 100-200mL.

Flies expressing *hAPP* displayed a high percent of flies that landed at the 300mL mark and above. About 59% of standard-vial flies landed at 300mL and above while 41% of the flies landed below 300mL. In the siliconized-vial flies, 62.2% of flies landed at 300mL and above and 37.8% landed below 300mL (fig. 27). The highest percent of flies, for both the standardized-vial and siliconized-vial flies, landed between 400-500mL. The lowest percent of flies for the standardized-vial flies landed between the 100-200mL mark whereas siliconized-vial flies displayed the lowest percent of flies between 200-300mL.

Flies expressing *PsnL²³⁷* displayed a high percent of flies at 300mL and above. Standard-vial flies displayed a percentage of 62.4% of flies that landed above the 300mL mark and 37.6% landed below the 300mL mark. About 53.2% of siliconized-vial flies above the 300mL and 46.8% of flies below the 300mL

mark (fig. 28). Standard-vial flies had the highest percent of flies between 500mL and above and the lowest percent of flies landed between 100-200mL.

Siliconized-vial flies had the highest percent of flies between 0-100mL and the lowest percent of flies between 200-300mL.

Flies coexpressing *hAPP x PsnL²³⁷* displayed a high percent of flies at 300mL and above. Standard-vial flies displayed a high percent between 300mL and above with 61.6% and a lowest percent of flies below 300mL with 38.4% (fig. 29). Siliconized-vial flies displayed a high percent of flies at 300mL and above with 61% and a 39% of flies below the 300mL mark. Flies landed primarily between 0-100mL for the standard-vial flies and a low percent of standard-vial flies landed between 200-300mL. Siliconized-vial flies show a high percentage of flies between 0-100mL and >500mL. The lowest percent of siliconized-vial flies was found between 100-200mL.

The standard-vial flight assay data of the *PsnL²³⁷* lines were compared on a graph (fig. 30). At 0-100mL, the *w¹¹⁸* control displayed the lowest percent of flies that landed while the highest percent of flies that landed were flies coexpressing *hAPPxPsnL²³⁷*. At 100-200mL, the *PsnL²³⁷* line displayed the lowest percent of flies that landed while flies expressing *hAPP* had the highest percent of flies that landed. At 200-300mL, flies expressing *hAPPxPsnL²³⁷* displayed the lowest percent of flies that landed while flies expressing *hAPP* had the highest percent of flies that landed. At 300-400mL, flies expressing *hAPP* displayed the lowest percent of flies that landed while the highest percent of flies

that landed were the w^{1118} control. At 400-500mL, flies expressing $PsnL^{237}$ displayed the lowest percent of flies that landed compared to w^{1118} that had the highest percent of flies that landed. At 500mL and above, flies expressing $hAPP$ displayed the lowest percent of flies that landed while flies expressing $PsnL^{237}$ had the highest percent of flies that landed.

The siliconized-vial flight assay data of the $PsnL^{237}$ lines were compared on a graph (fig.31). At 0-100mL, the w^{1118} control had the lowest percent of flies whereas flies expressing $PsnL^{237}$ displayed the highest percent of flies that landed. At 100-200mL, flies coexpressing $hAPPxPsnL^{237}$ had the lowest percent of flies that landed whereas flies expressing $hAPP$ displayed the highest percent of flies that landed. At 200-300mL, flies expressing $PsnL^{237}$ had the lowest percent of flies whereas flies expressing w^{1118} displayed the highest percent of flies that landed. At 300-400mL, flies expressing $PsnL^{237}$ displayed the lowest percent of flies whereas flies expressing $hAPP$ had the highest percent of flies that landed. At 400-500mL, flies expressing $PsnL^{237}$ displayed the lowest percent of flies that landed whereas the w^{1118} control had the highest percent of flies that landed. At 500mL and above, flies expressing $hAPP$ displayed the lowest percent of flies whereas flies coexpressing $hAPPxPsnL^{237}$ displayed the highest percent of flies that landed.

Overall, there was no particular pattern in both the standard-vial and siliconized-vial flight assays. The w^{1118} control displayed a gradual increase in

percent from 0mL to 500mL. A high percent of flies landed above 300mL for all of the genotypes.

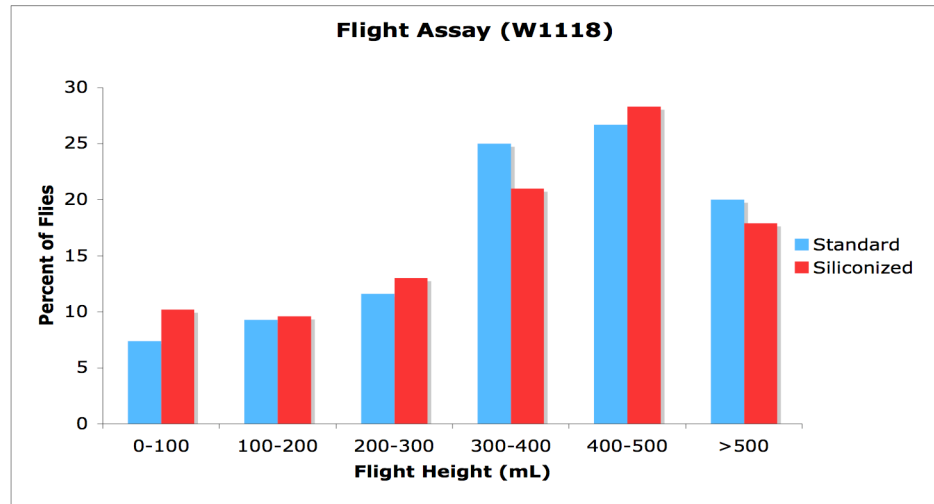


Figure 26. Flight Assay Result of the w^{1118} controls in Standard and Siliconized Vials

The greatest percentage of standard and siliconized samples scored at 400-500mL

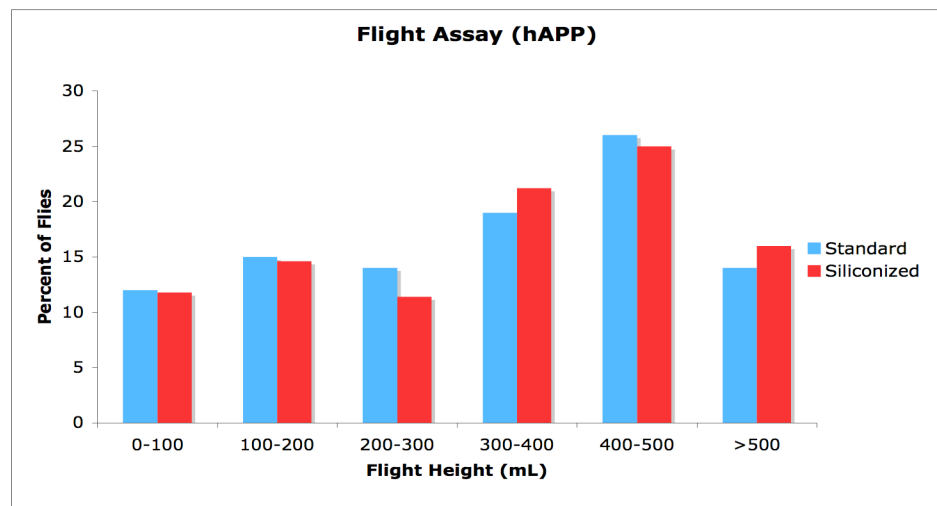


Figure 27. Flight Assay Result of $hAPP$ -expressing flies in Standard and Siliconized Vials

The greatest percentage of standard and siliconized samples scored at 400-500mL

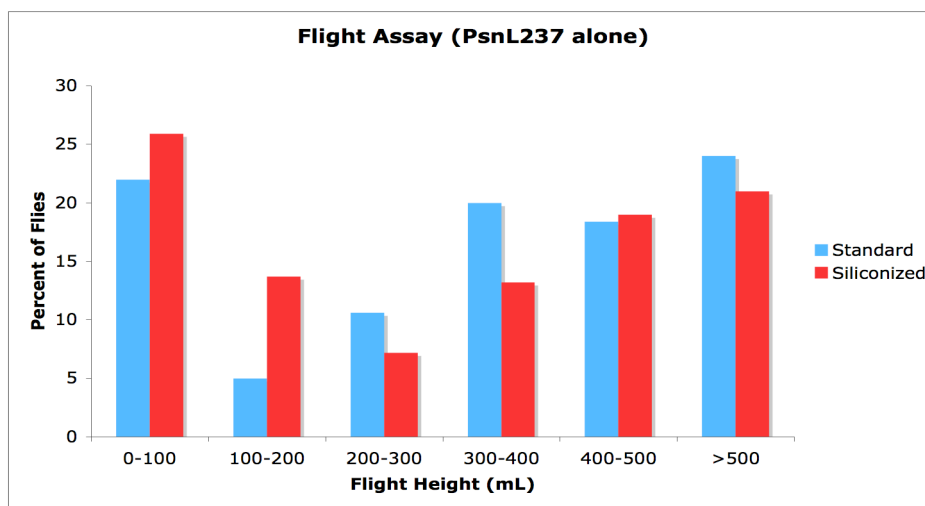


Figure 28. Flight Assay Result of *PsnL*²³⁷ in Standard and Siliconized Vials
The greatest percentage of siliconized samples scored at 0-100mL, and standard samples scored at >500 mL.

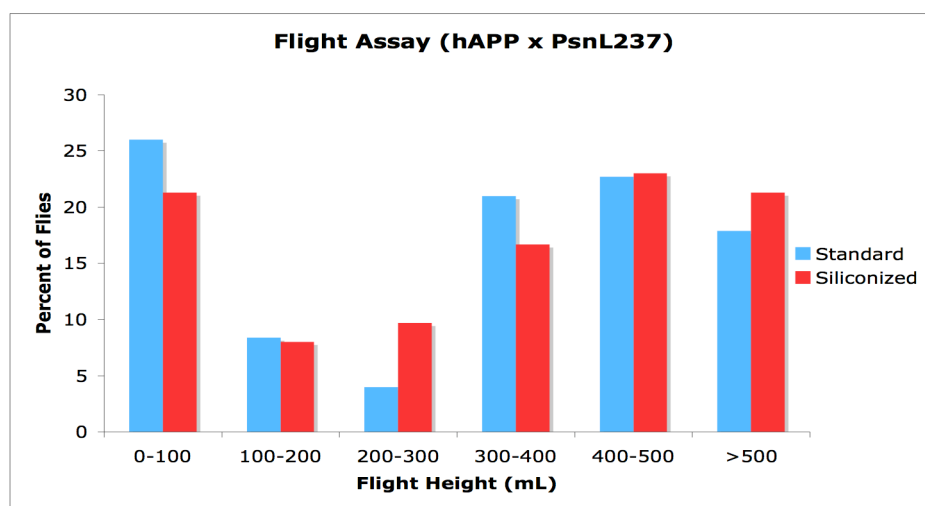


Figure 29. Flight Assay Result of flies coexpressing *hAPPxPsnL*²³⁷ in Standard and Siliconized-Vial flies
The greatest percentage of siliconized samples scored at 400-500mL, and standard samples scored between 0-100 mL.

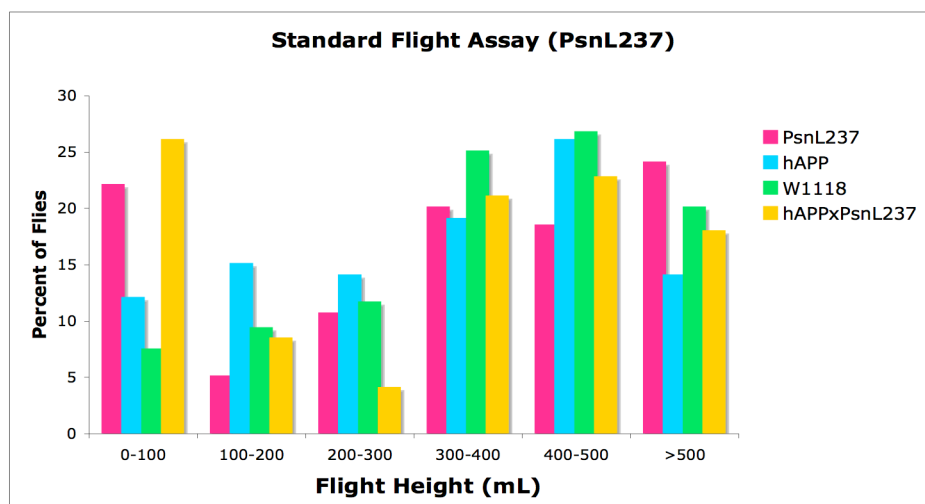


Figure 30. Standard climbing assay of $PsnL^{237}$, $hAPPxPsnL^{237}$, $hAPP$ and w^{1118}

The four genotypes show an inconsistent pattern. The w^{1118} control appears to increase in percent of flies every increment beginning at 0mL until 500mL.

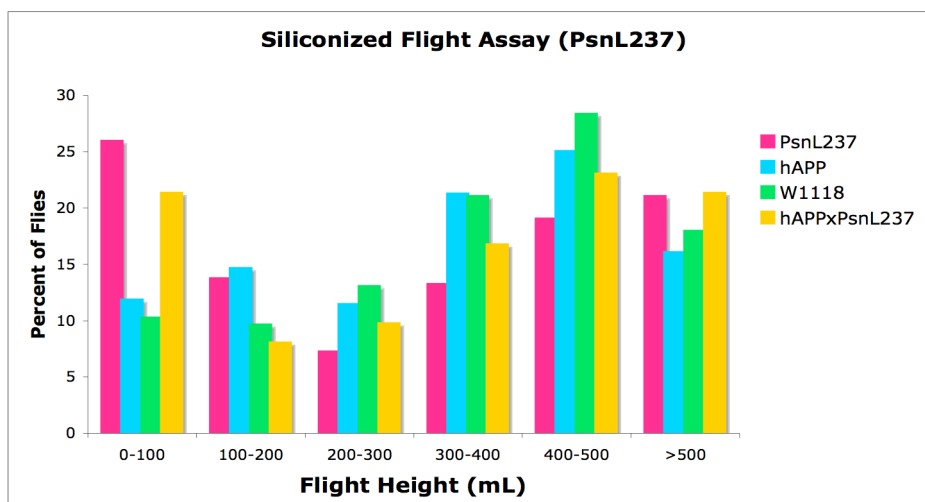


Figure 31. Standard climbing assay of $PsnL^{237}$, $hAPPxPsnL^{237}$, $hAPP$ and w^{1118}

The majority of flies landed at 300mL and above. The w^{1118} control shows a gradual increase in percent of flies starting from from 100mL to 500mL. All the other genotypes showed no particular pattern.

Transmission Electron Microscopy

To gain more insight into the age-dependent pathology of sIBM, we performed transmission electron microscopy on the w^{1118} control, flies expressing $PsnL^{237}$, and flies coexpressing $hAPPxPsnL^{237}$.

Flight muscle from 1-week old w^{1118} flies displayed intact sarcomeres and specific features in muscle fiber such as T tubules and sarcoplasmic reticulum (fig.32). Flight muscles from 3-week old flies also retained good muscle structure although there appeared to have been a loss of contractile elements, consistent with age-dependent muscle atrophy (fig.33).

The contractile apparatus within the flight muscles of $hAPP$ transgenic flies looked normal, with good Z-bands, sarcomere widths, and internal membrane systems. Flight muscles from 1-week old $hAPP$ -expressing flies contained large numbers of highly distorted mitochondria in the muscle fibers. Many were swollen and had lost their electron opacity, and instead looked ghost-like and empty. The cristae in the abnormal mitochondria were largely destroyed and the few that remained had lost their normal pattern of organization. It should be noted that at this age, the flies displayed defects in climbing behavior, suggesting that mitochondrial loss may not precede detectable changes in motor function. Flight muscles of 3-week old $hAPP$ -expressing flies revealed fiber necrosis with a loss of contractile elements, disrupted internal membrane systems, and reduced numbers of mitochondria.

Muscle fibers of 1-week old flies expressing *PsnL*²³⁷ looked normal and displayed well-developed sarcomeres as well as good Z-bands. Mitochondria appeared normal and no hint of mitochondrial dysfunction was present. Flight muscles of 3-week old flies showed similar results. Mitochondria appeared normal and the Z-bands, sarcomere widths, and internal membrane system appeared normal and intact.

In flies expressing *hAPPxPsnL*²³⁷, at 1-week, muscle fibers present normal sarcomere widths, sarcoplasmic reticulum, and Z-bands. Mitochondria look normal and exhibit no changes. After 3 weeks, no changes are visible in the muscle samples.

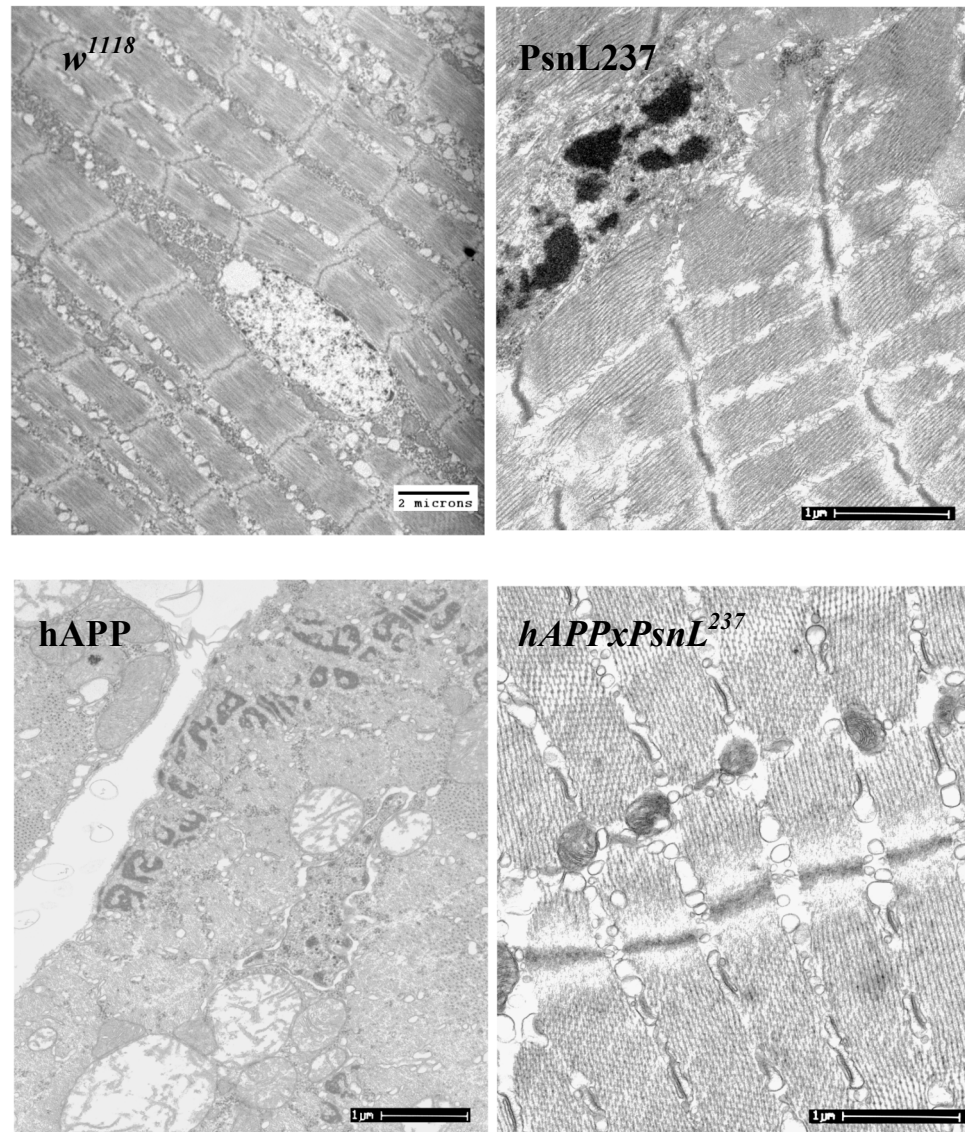


Figure 32. Transmission electron micrograph of w^{1118} , $PsnL^{237}$, $hAPP$, and $hAPPxPsnL^{237}$ at 1 week

Micrographs of tergoprothoracic muscles in *Drosophila*, which indicate the presence of mitochondrial defects in $hAPP$ -expressing flight muscles. The white circular spheres in the muscle are mitochondria that have become defective. All other genotypes show no signs of mitochondrial damage.

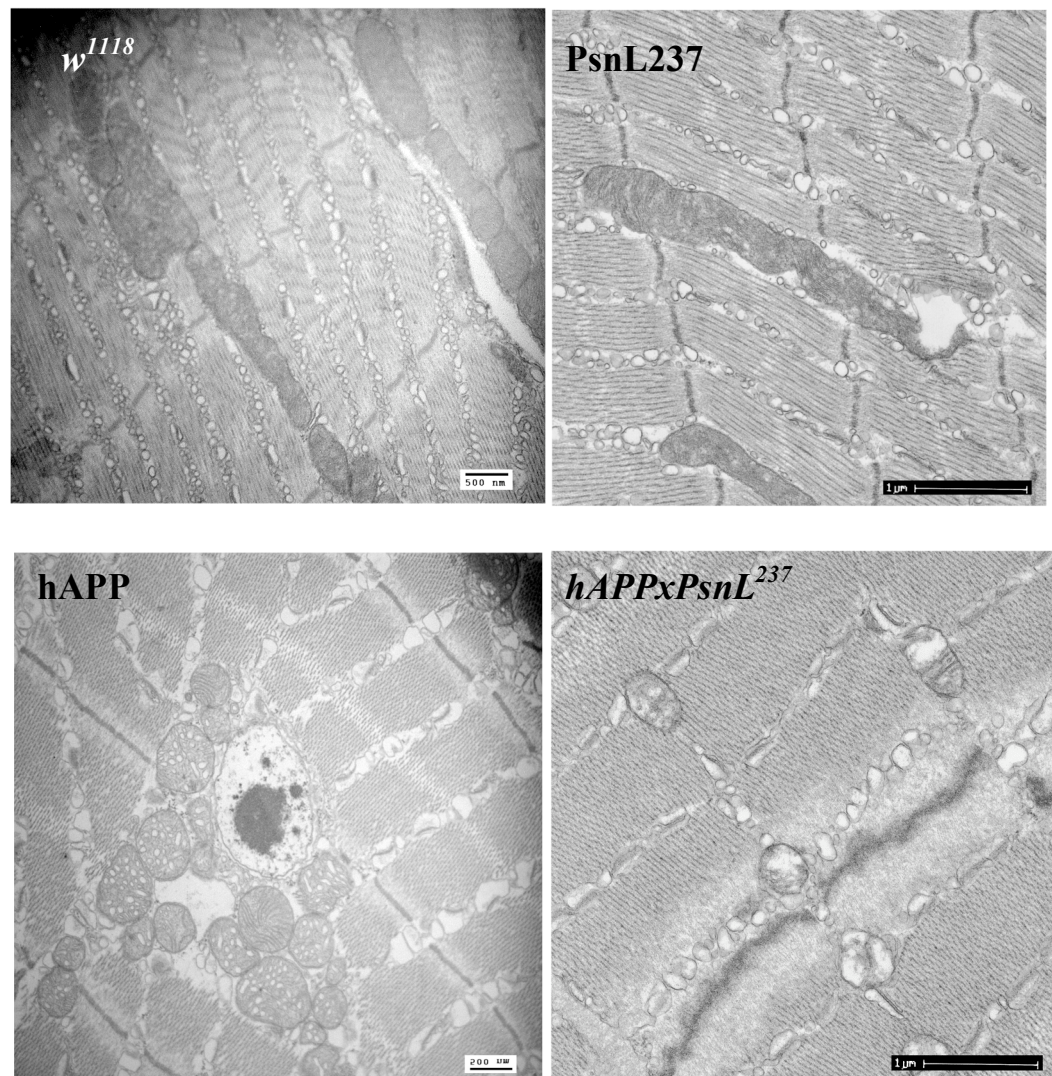


Figure 33. Transmission electron micrograph of w^{1118} , $PsnL^{237}$, $hAPP$, and $hAPPxPsnL^{237}$ at 3 weeks

Micrographs of tergoprochanteral muscles in *Drosophila* showing an increase in mitochondria that are defective in $hAPP$ -expressing flight muscles. The mitochondria seem translucent and deteriorating. All other genotypes show normal muscle fiber features and no signs of mitochondrial damage.

DISCUSSION

Sporadic-Inclusion Body Myositis affects 35 patients per million in people older than 50 years. Limited knowledge about factors that lead to this progressive muscle disease has prevented possible discoveries for successful therapeutic treatments. Analysis of muscle biopsies from sIBM patients has established possible candidates responsible for sIBM, including: APP, oxidative stress, endoplasmic reticulum (ER) stress, mitochondrial defects, inflammation and accumulation of free cholesterol (Schwartz, unpublished). Unfortunately, since these samples were collected after the onset of symptoms, analysis of possible targets involved in the pathogenesis of sIBM have been hard to establish.

A candidate that has gained popularity in the research of Alzheimer's disease and IBM-like disorders is the abnormal expression of APP. Patients with sIBM have inclusion bodies rich in APP in their muscle cells, which has directed researchers to focus on the causes of such pathological features. Transgenic studies with mouse models have supported this hypothesis where the expression of hAPP in skeletal muscles showed symptoms similar to patients with sIBM (Sugarman *et al.*, 2000). The short lifespan of *D. melanogaster* is an intrinsic property for studying neurodegenerative diseases since results are acquired faster compared to mouse models. Engineering flies that express human APP demonstrates the ability to model flies expressing neurodegenerative diseases that share similar characteristics in humans.

In this research, a complementary model for sIBM using transgenic flies was produced to express hAPP and mutant presenilin in the skeletal muscles. In preliminary studies, transgenic flies expressing *hAPP* displayed progressive muscle weakness and behavioral changes similar to humans. By using the fly system, I was able to show interaction between mutant presenilin and hAPP under various environmental factors.

The goal of the research was to find a protein that interacted with human APP during muscle degeneration and determine whether coexpression alleviated or exacerbated the symptoms. I used climbing assays to evaluate the extent to which symptoms occurred. The results suggest that in standard and siliconized environments, the coexpression of presenilin and hAPP in flies alleviated symptoms caused by APP alone. These results did not support my hypothesis. My findings indicate that particular mutations in presenilin may have contradictory effects on the abnormal expression of APP. Previous studies have linked presenilin function with exacerbated symptoms. Wolfe and colleagues have indicated that mutant presenilins cause an unusual “gain of function” and “loss of function”, resulting in increased levels of A β 42 and a decrease in proteolytic activity.

Use of Climbing Assays to evaluate hAPP and mutant presenilin interaction

The goal of the research was addressed through the comparison of climbing assay results of flies coexpressing hAPP and mutant presenilin to the w^{1118} control and hAPP-expressing flies. Detailed analysis of the climbing assays among the four genotypes revealed a strong relationship between presenilin and flies coexpressing hAPP and mutant presenilin. The results of the climbing and flight assays indicate that coexpression of presenilin and hAPP in flies suppressed degeneration caused by APP expression alone. The data show that the two different presenilin alleles had differential effects on climbing ability and in flight assay behavior. The w^{1118} controls in the climbing assays had a higher percent of flies successfully climbing compared to the *hAPP* lines. Flies expressing *hAPP* displayed the lowest climbing ability among all the genotypes. This verifies that the expression of *hAPP* in the muscles causes symptoms of muscle degeneration as seen in patients with sporadic-Inclusion Body Myositis. In addition, failure to climb was not due to a loss in the negative geotropism but the apparent lack of strength to hold to the surface of the vial.

The expression of mutant presenilin alone in the muscle cells resulted in lower climbing ability than the w^{1118} control but higher than the flies expressing *hAPP*. In flies only expressing the mutant presenilin genotype, proteolytic processing in *Drosophila* is of the APP homolog. Studies have shown that proteolytic processing of the APP homolog in *Drosophila* differs from processing

of APP in humans. In *Drosophila*, amyloid-related proteins are not generated as a byproduct of proteolysis. Furthermore, a mutation in presenilin can decrease proteolytic activity, which accounts for the gradual decrease in climbing ability. An additional player that influences the decrease in climbing ability is the natural biological properties of aging. Surprisingly, *PsnE*²⁸⁰ displays a percent of successful climb lower than *hAPP* at three and four weeks. These findings may suggest that the expression of *PsnE*²⁸⁰ is lethal, since a number of flies died at three weeks upon doing the experiments. Another assumption would be that presenilin may exacerbate muscle degeneration.

Interestingly, during the third week, a decrease in climbing ability occurs in *PsnE*²⁸⁰ and *PsnL*²³⁷ standard-vial flies. Since presenilin is part of the γ -secretase complex, which is responsible for the proteolysis of APP and other transmembrane proteins in signaling, an expression of the mutant presenilin will decrease γ -secretase activity in cell signaling and thus display a decrease in climbing ability. Furthermore, transmission electron microscopy was carried out to examine any phenotypic changes in muscles fibers. Micrographs demonstrate the lack of defective mitochondria or apoptotic characteristics in standard-vial *PsnL*²³⁷ flies. This suggests that the lack of amyloid-related proteins in the muscle cells is not causing the gradual degeneration found in the climbing assays. It is possible that factors responsible for the degeneration of the muscle cells may lie in the decrease in proteolytic activity prompted by mutant presenilin.

In contrast, in the siliconized-vial environment, flies expressing *PsnE*²⁸⁰ and *PsnL*²³⁷ appear to increase in climbing ability at three weeks. Stress caused by excessive work to climb up a very smooth surface may contribute to an overexpression of the mutant presenilin genes, which lead to an increase in climbing ability. The overexpression of mutant presenilin may be caused by the overuse of muscle activity, which in turn may have briefly increased cell metabolism, inadvertently increasing proteolytic activity. The increase is later followed by a decrease at four weeks. This indicates that the cells had reached their limit and could no longer expend such energy.

Flies coexpressing *hAPP* and *Psn* displayed similar characteristics to flies expressing presenilin alone in the muscle cells. Climbing ability was lower in percentage than the *w*¹¹⁸ control but higher in climbing ability than the flies expressing *hAPP*. In climbing assays, *hAPPxPsn* has demonstrated a higher percent in climbing ability compared to flies expressing mutant presenilin. This suggests that expression of mutant presenilin has a strong effect on the behavior of the flies coexpressing *hAPP* and mutant presenilin. The climbing ability of *hAPP* and *Psn* over four weeks share a close trend to the *w*¹¹⁸ control although climbing ability is lower than the wildtype. In flies coexpressing *hAPPxPsnE*²⁸⁰, flies in the standard-vial assay appear to decrease in climbing ability relative to the *w*¹¹⁸ control. At four weeks, the flies show a further decrease in climbing ability. This data suggests that *PsnE*²⁸⁰ may play a key role in suppressing degeneration in the muscle cells. This particular mutation may cause the protein

to regulate APP proteolysis so that it is normal. The slight decrease in climbing ability after three weeks may be a result of age-dependent degeneration.

In the siliconized-vial assay, flies expressing *hAPPxPsnE²⁸⁰* show a decrease at three weeks. A plausible explanation is that the added stress from the environment may have lowered the efficiency of the mutants role to suppress degeneration. Our data suggests that excessive work exacerbates the underlying pathology. Schwartz and colleagues demonstrated that extra work caused by a smoother surface in siliconized vials, would increase the mechanical stress on muscle fibers and contribute to muscle damage. Although climbing ability was not drastic, data suggests that muscle activity at three weeks was decreased due to an increase production of A β peptides by mutant presenilin. It is also possible that aging may be greatly affected and be another contributive factor to the decrease in climbing ability. At 4 weeks, climbing ability increases in *hAPPxPsnE²⁸⁰*.

The behavior of flies coexpressing *hAPPxPsnL²³⁷* seems to contradict the results with flies coexpressing *hAPPxPsnE²⁸⁰*. It is plausible that mutations in certain alleles on presenilin may result in varies behavior suggesting that the two mutations on presenilin may have opposite effects when interacting with *hAPP*. In the standard-vial assay, data shows that flies coexpressing *hAPP* and *PsnL²³⁷* show a decrease in climbing ability at week 2 and 3. At week 4, an increase in climbing ability occurs. These findings suggest that *PsnL²³⁷* may exacerbate the symptoms of degeneration, these effects correlate with the behavior exhibited by

flies coexpressing hAPP and mutant presenilin. Interestingly, flies expressing *hAPP* and *PsnL²³⁷* have a higher percent of successful climb than flies expressing *PsnL²³⁷* at four weeks. In the siliconized-vial assay, flies coexpressing *hAPP* and *PsnL²³⁷* drop in climbing ability during the second week, increase in climbing ability at three weeks, and decreases again after four weeks with a percent of successful climb higher than flies expressing *PsnL²³⁷*. This data shows that a siliconized-vial environment does indeed have profound effects on the interaction between *hAPPxPsn*. The coexpression of *hAPP* and *PsnL²³⁷* in flies, in a siliconized-vial environment, may influence the characteristics of *PsnL²³⁷* function. From the first week onto the second week, *PsnL²³⁷* may be participating in abnormal APP proteolysis. Interestingly, the increase in climbing ability may be due to increased muscle activity where flies try to make up for the degeneration in their muscles by climbing harder. At four weeks, flies coexpressing *hAPPxPsnL²³⁷* eventually demonstrate a higher percent of successful climb than *PsnL²³⁷*. Flies have lost their ability to fully hold on to the sides of the vial, yet the flies coexpressing *hAPPxPsnL²³⁷* do better than the other genotypes.

Flight Assays to evaluate muscle activity

The flight assay differs from the climbing assay in that it does not measure both the muscle and age-dependent interactions but instead endeavors to analyze the extent of degeneration in flight muscles. Flight assay results for both alleles, in siliconized and standard-vial environment displayed inconsistency and variation in mutant presenilin, *hAPP*, and flies coexpressing hAPP and Psn. A trend was set by the w^{1118} control. The w^{1118} control displayed an increase after every increment from the lowest (0mL) to highest (500mL). To assess the flight assay, flies that landed at higher increments meant that flight capabilities had not been affected by muscle degeneration from the climbing assays. Flies that landed at lower increments proposed that those flies had lost their flying ability.

The majority of the genotypes had a high percentage of flies above 300mL. This data suggests that all the genotypes possessed good flying capabilities after four weeks of climbing activity. Flies found below the 100mL mark may be a result of complications in flight muscles, which may have undergone extensive degeneration. The *PsnE²⁸⁰* flight assay shows that all genotypes reared in siliconized vials, had a higher percent in flies that landed above 300mL than the standard-vial flies, whereas in the *PsnL²³⁷* flight assay, standard-vial flies shared a higher percent in flies that landed above the 300mL mark.

The results overall revealed that all the genotypes had high percentages of flies above 300mL and above. This suggests that muscle degeneration in

climbing activity have no significance to flight ability. Genotypes that did poorly in the climbing assays showed better results in the flight assays.

Transmission Electron Microscopy to examine changes in muscle fiber

In order to understand muscle degeneration, transmission electron microscopy was carried on to look for any changes due to degeneration. Flies that were evaluated were the *w¹¹¹⁸* control, flies expressing *PsnL²³⁷*, flies coexpressing *hAPPxPsnL²³⁷*, and *hAPP*-expressing flies. The flies were examined at 1 week and 3 weeks.

During the first week, the *w1118* control displayed well-developed sarcomeres and associated internal membrane systems such as T-tubules and sarcoplasmic reticulum. Flight muscles of the *w1118* control at 3 weeks showed intact muscle structure although there appeared to be evidence of age-dependent atrophy. Flight muscles of *PsnL²³⁷* and flies coexpressing *hAPPxPsnL²³⁷* in week 1 and 3 display no abnormal changes. Sarcomeres, mitochondria, and sarcoplasmic reticulum looked intact and normal. On the other hand, *hAPP*-expressing flies displayed abnormal changes at week 1. The contractile apparatus of flies expressing *hAPP* looked normal, with good Z bands, sarcomere width, and internal membrane systems. Among the well-developed sarcomeres, muscle fibers contained large numbers of highly distorted mitochondria. The appearance

of those mitochondria was empty and swollen. These abnormal phenotypes precede detectable change in motor function, which suggests that mitochondrial loss precedes defects in climbing and flight behavior. At 3 weeks, the muscle fiber still shows normal fibers but present a few abnormal changes such as necrosis of some muscle fiber and an increase in defective mitochondria. Organization in the mitochondria seemed distorted as well as the formation of the cristae. The observations of mitochondrial loss in hAPP-expressing flies would be expected to reduce in ATP production and other pathways, as well as affect climbing and flight ability.

The use of transmission electron microscopy is a good tool for learning about the phenotypic changes in the muscle fibers. The presence of mitochondrial defects at early stages of development in *hAPP*-expressing flies allows us to further investigate the cause of early mitochondrial dysfunction and the pathways that are interrupted because of the defect.

Conclusion

In conclusion, my project explored the interaction between hAPP and mutant presenilin in two respective environments. My results indicate that flies coexpressing hAPP and mutant presenilin suppress the muscle degeneration seen in flies expressing hAPP alone. The use of *D. melanogaster* as a model is beneficial for the study of degenerative diseases like sIBM. My experimental results are a contribution to the advancement of understanding the pathogenesis of sIBM and eventually lead us closer to possible treatment of sIBM.

LITERATURE CITED

- Adams, M. D., *et al.* 2000. The genome sequence of *Drosophila melanogaster*. *Science* 287: 2185-2195.
- Antoniou, A. N., S. J. Powis, and T. Elliott. 2003. Assembly and export of MHC class I peptide ligands. *Current Opinion in Immunology* 15, (1) (Feb): 75-81.
- Ashburner, M., and C. M. Bergman. 2005. *Drosophila melanogaster*: A case study of a model genomic sequence and its consequences. *Genome Research* 15, (12) (Dec): 1661-7.
- Askanas, V., and W. K. Engel. 2007. Inclusion-body myositis, a multifactorial muscle disease associated with aging: Current concepts of pathogenesis. *Current Opinion in Rheumatology* 19, (6) (Nov): 550-9.
- Askanas, V., and W. K. Engel. 2001. Inclusion-body myositis: Newest concepts of pathogenesis and relation to aging and alzheimer disease. *Journal of Neuropathology and Experimental Neurology* 60, (1) (Jan): 1-14.
- Bonini, N. M., and M. E. Fortini. 2003. Human neurodegenerative disease modeling using drosophila. *Annual Review of Neuroscience* 26, : 627-56.
- Brown, S. T., R. P. Johnson, R. Senaratne, and I. M. Fearon. 2004. Amyloid beta peptides mediate physiological remodelling of the acute O₂ sensitivity of adrenomedullary chromaffin cells following chronic hypoxia. *Cardiovascular Research* 64, (3) (Dec 1): 536-43.
- Busciglio, J., A. Pelsman, C. Wong, G. Pigino, M. Yuan, H. Mori, and B. A. Yankner. 2002. Altered metabolism of the amyloid beta precursor protein is associated with mitochondrial dysfunction in down's syndrome. *Neuron* 33, (5) (Feb 28): 677-88.
- Cao, X., and T. C. Sudhof. 2004. Dissection of amyloid-beta precursor protein-dependent transcriptional transactivation. *The Journal of Biological Chemistry* 279, (23) (Jun 4): 24601-11.

- Crosby, M. A., J. L. Goodman, V. B. Strelets, P. Zhang, W. M. Gelbart, and FlyBase Consortium. 2007. FlyBase: Genomes by the dozen. *Nucleic Acids Research* 35, (Database issue) (Jan): D486-91.
- Dalakas, M. C.. 2006. Sporadic inclusion body myositis--diagnosis, pathogenesis and therapeutic strategies. *Nature Clinical Practice.Neurology* 2, (8) (Aug): 437-47.
- Danial, N. N., and S. J. Korsmeyer. 2004. Cell death: Critical control points. *Cell* 116, (2) (Jan 23): 205-19.
- Fossgreen, A., B. Bruckner, C. Czech, C. L. Masters, K. Beyreuther, and R. Paro. 1998. Transgenic drosophila expressing human amyloid precursor protein show gamma-secretase activity and a blistered-wing phenotype. *Proceedings of the National Academy of Sciences of the United States of America* 95, (23) (Nov 10): 13703-8.
- Halligan, D. L., and P. D. Keightley. 2006. Ubiquitous selective constraints in the drosophila genome revealed by a genome-wide interspecies comparison. *Genome Research* 16, (7) (Jul): 875-84.
- Hervias, I., M. F. Beal, and G. Manfredi. 2006. Mitochondrial dysfunction and amyotrophic lateral sclerosis. *Muscle & Nerve* 33, (5) (May): 598-608.
- Isoo, N., C. Sato, H. Miyashita, M. Shinohara, N. Takasugi, Y. Morohashi, S. Tsuji, T. Tomita, and T. Iwatsubo. 2007. Abeta42 overproduction associated with structural changes in the catalytic pore of gamma-secretase: Common effects of pen-2 N-terminal elongation and fenofibrate. *The Journal of Biological Chemistry* 282, (17) (Apr 27): 12388-96.
- Jayaraman, M., G. Kannayiram, and J. Rajadas. 2008. Amyloid toxicity in skeletal myoblasts: Implications for inclusion-body myositis. *Archives of Biochemistry and Biophysics* (Mar 26).
- Kimberly, W. T., M. J. LaVoie, B. L. Ostaszewski, W. Ye, M. S. Wolfe, and D. J. Selkoe. 2003. Gamma-secretase is a membrane protein complex comprised of presenilin, nicastrin, aph-1, and pen-2. *Proceedings of the National*

Academy of Sciences of the United States of America 100, (11) (May 27): 6382-7.

- Kozopas, K. M., C. H. Samos, and R. Nusse. 1998. DWnt-2, a drosophila wnt gene required for the development of the male reproductive tract, specifies a sexually dimorphic cell fate. *Genes & Development* 12, (8) (Apr 15): 1155-65.
- Kwong, L. K., and R. S. Sohal. 2002. Tissue-specific mitochondrial production of H₂O₂: Its dependence on substrates and sensitivity to inhibitors. *Methods in Enzymology* 349, : 341-6.
- Lilly, B., S. Galewsky, A. B. Firulli, R. A. Schulz, and E. N. Olson. 1994. D-MEF2: A MADS box transcription factor expressed in differentiating mesoderm and muscle cell lineages during drosophila embryogenesis. *Proceedings of the National Academy of Sciences of the United States of America* 91, (12) (Jun 7): 5662-6.
- Luo, W. J., H. Wang, H. Li, B. S. Kim, S. Shah, H. J. Lee, G. Thinakaran, T. W. Kim, G. Yu, and H. Xu. 2003. PEN-2 and APH-1 coordinately regulate proteolytic processing of presenilin 1. *The Journal of Biological Chemistry* 278, (10) (Mar 7): 7850-4.
- Madsen, L. B., B. Thomsen, K. Larsen, C. Bendixen, I. E. Holm, M. Fredholm, A. L. Jorgensen, and A. L. Nielsen. 2007. Molecular characterization and temporal expression profiling of presenilins in the developing porcine brain. *BMC Neuroscience* 8, (Sep 13): 72.
- Needham, M., and F. L. Mastaglia. 2008. Sporadic inclusion body myositis: A continuing puzzle. *Neuromuscular Disorders : NMD* 18, (1) (Jan): 6-16.
- Nunan, J., and D. H. Small. 2000. Regulation of APP cleavage by alpha-, beta- and gamma-secretases. *FEBS Letters* 483, (1) (Oct 13): 6-10.
- Oldfors, A., and C. Lindberg. 2005. Diagnosis, pathogenesis and treatment of inclusion body myositis. *Current Opinion in Neurology* 18, (5) (Oct): 497-503.

- Ponting C.P., Hutton M., Nyborg A., Baker M., Jansen K., and Golde T.E. (2001) Identification of a Novel Family of Presenilin Homologues. *Human Molecular Genetics* **11**(9), 1037-1044
- Reiter, L. T., L. Potocki, S. Chien, M. Gribskov, and E. Bier. 2001. A systematic analysis of human disease-associated gene sequences in drosophila melanogaster. *Genome Research* **11**, (6) (Jun): 1114-25.
- Rosen, D. R., L. Martin-Morris, L. Q. Luo, and K. White. 1989. A drosophila gene encoding a protein resembling the human beta-amyloid protein precursor. *Proceedings of the National Academy of Sciences of the United States of America* **86**, (7) (Apr): 2478-82.
- Schwartz L., Woodard C. Unpublished
- Seidner, G. A., Y. Ye, M. M. Faraday, W. G. Alvord, and M. E. Fortini. 2006. Modeling clinically heterogeneous presenilin mutations with transgenic drosophila. *Current Biology : CB* **16**, (10) (May 23): 1026-33.
- Selkoe, D.J.(2001) Presenilin, Notch, and the Genesis and Treatment of Alzheimer's Disease. *Proc. Natl. Acad. Sci. USA* **98** (20), 11039-11041
- Sisodia, S. S., S. H. Kim, and G. Thinakaran. 1999. Function and dysfunction of the presenilins. *American Journal of Human Genetics* **65**, (1) (Jul): 7-12.
- Storey, E., and R. Cappai. 1999. The amyloid precursor protein of alzheimer's disease and the abeta peptide. *Neuropathology and Applied Neurobiology* **25**, (2) (Apr): 81-97.
- Strazielle, C., M. Dumont, K. Fukuchi, and R. Lalonde. 2004. Transgenic mice expressing the human C99 terminal fragment of betaAPP: Effects on cytochrome oxidase activity in skeletal muscle and brain. *Journal of Chemical Neuroanatomy* **27**, (4) (Jul): 237-46.
- Strooper, B. D., and W. Annaert. 2001. Presenilins and the intramembrane proteolysis of proteins: Facts and fiction. *Nature Cell Biology* **3**, (10) (Oct): E221-5.

- Sugarman, M. C., T. R. Yamasaki, S. Oddo, J. C. Echevoyen, M. P. Murphy, T. E. Golde, M. Jannatipour, M. A. Leissring, and F. M. LaFerla. 2002. Inclusion body myositis-like phenotype induced by transgenic overexpression of beta APP in skeletal muscle. *Proceedings of the National Academy of Sciences of the United States of America* 99, (9) (Apr 30): 6334-9.
- Tabaton, M., and E. Tamagno. 2007. The molecular link between beta- and gamma-secretase activity on the amyloid beta precursor protein. *Cellular and Molecular Life Sciences : CMLS* 64, (17) (Sep): 2211-8.
- Takasugi, N., T. Tomita, I. Hayashi, M. Tsuruoka, M. Niimura, Y. Takahashi, G. Thinakaran, and T. Iwatsubo. 2003. The role of presenilin cofactors in the gamma-secretase complex. *Nature* 422, (6930) (Mar 27): 438-41.
- Tandon, A., and P. Fraser. 2002. The presenilins. *Genome Biology* 3, (11) (Oct 23): reviews3014.
- Thinakaran, G.. 1999. The role of presenilins in alzheimer's disease. *The Journal of Clinical Investigation* 104, (10) (Nov): 1321-7.
- Thompson, J. N., Jr, M. Ashburner, and R. C. Woodruff. 1977. Presumptive control mutation for alcohol dehydrogenase in drosophila melanogaster. *Nature* 270, (5635) (Nov 24): 363.
- Turner, P. R., K. O'Connor, W. P. Tate, and W. C. Abraham. 2003. Roles of amyloid precursor protein and its fragments in regulating neural activity, plasticity and memory. *Progress in Neurobiology* 70, (1) (May): 1-32.
- Wang, H., W. J. Luo, Y. W. Zhang, Y. M. Li, G. Thinakaran, P. Greengard, and H. Xu. 2004. Presenilins and gamma-secretase inhibitors affect intracellular trafficking and cell surface localization of the gamma-secretase complex components. *The Journal of Biological Chemistry* 279, (39) (Sep 24): 40560-6.
- Wing, J. P., B. A. Schreader, T. Yokokura, Y. Wang, P. S. Andrews, N. Huseinovic, C. K. Dong, et al. 2002. *Drosophila morgue* is an F

box/ubiquitin conjugase domain protein important for grim-reaper mediated apoptosis. *Nature Cell Biology* 4, (6) (Jun): 451-6.

Wolfe, M. S., W. Xia, B. L. Ostaszewski, T. S. Diehl, W. T. Kimberly, and D. J. Selkoe. 1999. Two transmembrane aspartates in presenilin-1 required for presenilin endoproteolysis and gamma-secretase activity. *Nature* 398, (6727) (Apr 8): 513-7.

Yagi, Y., S. Tomita, M. Nakamura, and T. Suzuki. 2000. Overexpression of human amyloid precursor protein in drosophila. *Molecular Cell Biology Research Communications : MCBRC* 4, (1) (Jul): 43-9.

Yang, D. S., A. Tandon, F. Chen, G. Yu, H. Yu, S. Arawaka, H. Hasegawa, et al. 2002. Mature glycosylation and trafficking of nicastrin modulate its binding to presenilins. *The Journal of Biological Chemistry* 277, (31) (Aug 2): 28135-42.

Yu, W. H., A. Kumar, C. Peterhoff, L. Shapiro Kulnane, Y. Uchiyama, B. T. Lamb, A. M. Cuervo, and R. A. Nixon. 2004. Autophagic vacuoles are enriched in amyloid precursor protein-secretase activities: Implications for beta-amyloid peptide over-production and localization in alzheimer's disease. *The International Journal of Biochemistry & Cell Biology* 36, (12) (Dec): 2531-40.